

A Thesis for the Degree of Ph.D. in Engineering

Study on CNN based Spine Estimator from Moire Image  
for Screening of Adolescent Idiopathic Scoliosis

August 2018

Graduate School of Science and Technology  
Keio University

CHOI Ran



---

# Contents

1. Introduction .....	1
1.1 Spinal structure .....	3
1.2 Adolescent idiopathic scoliosis .....	4
1.3 Diagnostic criterion of AIS, Cobb angle and angle of vertebral rotation: their significances and measurements .....	5
1.4 Screening step of AIS .....	8
1.4.1 International state of the spinal screening .....	9
1.5 Proposal .....	10
1.5.1 Outline of the thesis .....	14
1.5.2 Contributions of the thesis .....	15
2. Overview of the proposed system and related works .....	17

---

2.1	Overview of the proposed system .....	18
2.1.1	Dataset – Moire and X-ray images .....	18
2.1.2	Networks .....	20
2.1.3	Post-processing .....	22
2.2	Automatic measuring methods of two indicators, Cobb angle and AVR .....	22
2.2.1	The automatic measuring method of Cobb angle .....	23
2.2.2	Automatic measuring method for AVR .....	23
2.3	Spine screening methods and their evaluation .....	25
2.3.1	X-ray .....	25
2.3.2	CT .....	25
2.3.3	Ultrasound .....	27
2.3.4	Optical methods .....	28
2.3.5	Moire method .....	29
2.3.6	Machine learning based Moire method .....	30
2.3.7	Moire method using an image processing .....	30
2.2.8	Kinect .....	31
2.3.9	Adam’s forward bend test .....	32
2.2.10	Tool and smartphone application .....	32
3.	Generation methods for a dataset .....	35

---

3.1	Feature collection for the dataset .....	35
3.2	Dataset generation .....	37
3.2.1	Mergence method for two data sets .....	37
3.2.2	Evaluation of results used the different the mergence method .....	41
3.3	Dataset component .....	42
3.3.1	Component method for a dataset .....	42
3.3.2	Evaluation of results used the different component of datasets .....	43
3.3.3	Component ratio of patients in the dataset .....	46
3.3.4	Evaluation of component ratio of patients in a dataset .....	48
3.4	Conclusion of the dataset .....	50

## 4.Measurement methods of Cobb angle and of AVR...51

4.1	Proposed Method for measuring Cobb angle .....	51
4.1.1	Validation of the proposed Cobb method .....	56
4.1.2	Limitation of the proposed Cobb method .....	60
4.2	Proposed method for measuring AVR .....	60
4.2.1	Dataset for the spinal modeling .....	61
4.2.2	Validation of the proposed AVR method .....	63

---

5. Spine Estimation from moire image.....	67
5.1 Networks of CNN.....	67
5.1.1 Network structure to estimate the spine .....	69
5.2 Dataset .....	70
5.3 Result evaluation .....	70
5.3.1 Evaluation using the proposed method measuring Cobb angle .....	77
5.3.2 Evaluation using the proposed method measuring AVR .....	78
5.4 Conclusions of experiments .....	83
6. Conclusion.....	85
Acknowledgment.....	97

---

# List of figures

<b>Figure 1-1</b>	Spinal structure at three different views.....	3
<b>Figure 1-2</b>	Measurement of Cobb angle .....	6
<b>Figure 1-3</b>	2D method for measuring AVR ( $\theta$ ) .....	7
<b>Figure 1-4</b>	3D method for measuring AVR ( $\theta$ ) .....	7
<b>Figure 1-5</b>	Steps of the spinal screening by moire method .....	9
<b>Figure 1-6</b>	The process of proposed spine estimator .....	12
<b>Figure 1-7</b>	Surface deformations by the rotated spines .....	13
<b>Figure 1-8</b>	Moire patterns and x-ray images in accordance with each deformity .....	13
<b>Figure 2-1</b>	The environment for a Moire screening.....	18
<b>Figure 2-2</b>	The collected data.....	19
<b>Figure 2-3</b>	The Network for training.....	21
<b>Figure 2-4</b>	The Network for evaluation. ....	21
<b>Figure 2-5</b>	Architecture of CNN .....	22
<b>Figure 2-6</b>	An overview of method using DNN .....	24

---

<b>Figure 2-7</b>	An overview of fully automatic method .....	24
<b>Figure 2-8</b>	Ultrasound method.....	27
<b>Figure 2-9</b>	Optical method, Fometric 3D.....	28
<b>Figure 2-10</b>	A Moire equipment and a Moire image obtained from the Moire machine.....	29
<b>Figure 2-11</b>	A Moire method using an image processing.....	30
<b>Figure 2-12</b>	Screening of AIS using Kinect .....	31
<b>Figure 2-13</b>	Adam’s forward bend test.....	32
<b>Figure 2-14</b>	Smartphone application .....	33
<b>Figure 3-1</b>	The collected data from X-ray image.....	36
<b>Figure 3-2</b>	Merging process based on the silhouette.....	38
<b>Figure 3-3</b>	Poorly fitted spinal position .....	38
<b>Figure 3-4</b>	Methods for merging two images .....	39
<b>Figure 3-5</b>	Merged results.....	40
<b>Figure 3-6</b>	The used features in five datasets .....	43
<b>Figure 3-7</b>	Comparison among MAEs of each dataset .....	44
<b>Figure 3-8</b>	Estimation results .....	45
<b>Figure 3-9</b>	Graphs of frequencies .....	47
<b>Figure 3-10</b>	Results trained using datasets generated with balance, and generated randomly ..	49
<b>Figure 4-1</b>	Comparison the conventional method with the conventional method .....	52
<b>Figure 4-2</b>	Proposed method of measuring Cobb angle .....	53
<b>Figure 4-3</b>	Curve fittings .....	55
<b>Figure 4-4</b>	Center position of vertebral body .....	55
<b>Figure 4-5</b>	Cobb angle comparison .....	56

---

<b>Figure 4-6</b>	Correlation (top) and Bland-Altman plot (bottom) between Cobb angles measured by doctors and by the proposed method.....	58
<b>Figure 4-7</b>	The worst results when comparing two Cobb angles obtained by a doctor (right) and the proposed method (left) .....	59
<b>Figure 4-8</b>	3D method and 2D method for measuring AVR .....	61
<b>Figure 4-9</b>	One center point of vertebral body and one tip of spinous process collected from CT image slice .....	62
<b>Figure 4-10</b>	Spinal dimension of each vertebra .....	63
<b>Figure 4-11</b>	MAE and Average absolute AVR of each vertebra.....	65
<b>Figure 4-12</b>	Correlation (top) and Bland-Altman plot (bottom) between the proposed method and 3D AVR method .....	66
<b>Figure 5-1</b>	Architecture of CNN used in this thesis.....	68
<b>Figure 5-2</b>	Input images for the first and second CNNs.....	69
<b>Figure 5-3</b>	Estimated result of the normal spine .....	73
<b>Figure 5-4</b>	Estimated result of the spine with mild deformity .....	74
<b>Figure 5-5</b>	Estimated result of the spine with severe deformity .....	75
<b>Figure 5-6</b>	MAE of each features according to each vertebra .....	76
<b>Figure 5-7</b>	Correlation between two Cobb angles measured by Doctor and proposed method	78
<b>Figure 5-8</b>	MAE and average absolute AVR according to vertebra level. Here, the absolute AVR is an average angle of ground truth and estimated result.....	80
<b>Figure 5-9</b>	Correlation between Cobb angle and AVR .....	80
<b>Figure 5-10</b>	Patients having large AVR.....	81
<b>Figure 5-11</b>	Patients having small AVR .....	82
<b>Figure 5-12</b>	Results by specific Moire pattern of fat patients .....	84

## List of tables

<b>Table 1-1</b>	AIS treatment .....	5
<b>Table 1-2</b>	International state of the spinal screening .....	10
<b>Table 2-1</b>	Comparison of the convention screening methods .....	26
<b>Table 3-1</b>	The estimation result by according to the datasets .....	44
<b>Table 3-2</b>	Error of the datasets generated by different methods .....	41
<b>Table 3-3</b>	Frequency of dataset .....	47
<b>Table 3-4</b>	Result of two datasets .....	49
<b>Table 4-1</b>	Cobb angle error of the proposed method and comparison with another method.....	57
<b>Table 4-2</b>	MAE between the proposed method and 3D AVR method, and MAE in another reference between Ultrasound method and MRI method .....	65
<b>Table 5-1</b>	MAE of the estimated position.....	76
<b>Table 5-2</b>	MAE of Cobb angle of estimated position.....	77
<b>Table 5-3</b>	MAE of absolute AVR between the estimation petitions and the ground truth .....	80
<b>Table 5-4</b>	Result comparison with another method.....	83

# Chapter 1

## Introduction

Spinal screening is necessary for the early detection of spinal disease. Especially the periodic spinal screening of adolescent idiopathic scoliosis (AIS), a deformity characterized by an abnormal spinal curve with vertebral rotation (VR), is important for teenagers. It is because the abnormal curve progress rapidly while the growth stage, potentially becoming a serious disease [Batouche, 1992]. For diagnosing AIS, radiation methods such as X-ray and computed tomography (CT) are commonly used. On the other hand, for the periodic spinal screening, optical methods which do not carry the risk of radiation such as the integrated shape imaging system and the Formetric 3D, are used [Altaf et al., 2017, Kuroki, 2017].

The optical methods mainly measure the back surface of human to estimate the spine shape. They describe the spinal condition using surface metrics such as imbalances of the trunk, obtained from the spine shape and the back surface. They estimate the spine automatically, but require human intervention, i.e., the attachment of markers to anatomical landmarks. In

---

addition, they only can classify the spine as either normal or abnormal by the surface metrics which cannot diagnose the spine pathologically [Liu et al., 2003, Rankine et al., 2012, Patias et al., 2010]. Therefore, additional diagnosis by the radiation method is necessary to diagnosed as AIS in spite of the diagnosis of spinal deformity by the optical method.

In Japan, a Moire method is widely used for the early detection of AIS. This is an optical method to capture a Moire image by projecting a Moire pattern onto the back. The Moire image shows the curvature and depth of back surface like a contour line. By manual scoring of the symmetry level by checking for equal depth on the Morie image, the spine is classified as normal or abnormal. The Moire method, in common with other optical methods, has diagnostic limitation. [Takasaki 1970, Patias et al.,2010, Dentonet al, 1992]

X-ray is the most common method for pathologic diagnosis. The spine on the X-ray image is diagnosed based on the angle of the abnormal curve. The VR which is one symptom of AIS, is not used for the diagnosis of AIS but the progressing evaluation of AIS. The observer error ranges from 3° to 10° by manual measurement of the bent angle. Furthermore, feature identification for measurements of the VR and the bent angle, is a challenge by X-ray images of poor clarity. [Zhang et al., 2010]

CT is a method for pathologic diagnosis as well. It is a robust method from the image clarity due to 3D visualization of the spine by imaging technology. However, the feature identification for VR measurement, is also challenging because it is required the identification of vertebral apex on the 3D shape [Illés et al., 2011, Melhem at al., 2016].

Thus, both methods, optical and radiation, have the problems for the spinal screening. The optical methods have the diagnostic limitation by using surface metrics, and the radiation methods have a difficulty in measuring by requirement manual identification of features. If a screening method is non-radiative as well as capable of diagnosing pathologically, the number of use of the radiation method will be decreased during the spinal screening. In addition, this screening method can be used to monitor the AIS procession instead of the radiation methods.

Therefore, we propose a spine estimator for the spinal screening, that overcomes the difficulties of measurements and the diagnostic limitation of conventional screening methods. The proposed spine estimator automatically estimates the spine, and measures both angles, the bent angle and the VR, using the surface information for the pathologic diagnosis.

The spinal structure, diagnostic criterion of AIS and a general screening step for the spine are described preferentially from Section 1.1 to Section 1.4 for the better understanding of this thesis, and the proposed method is described in detail in Section 1.5.

## 1.1 Spinal structure

The bones that compose the spine are called a vertebra or a vertebral column. (a) in Figure 1-1 shows a side view of 17 vertebral columns consist of 12 thoracic and 5 lumbar vertebrae.

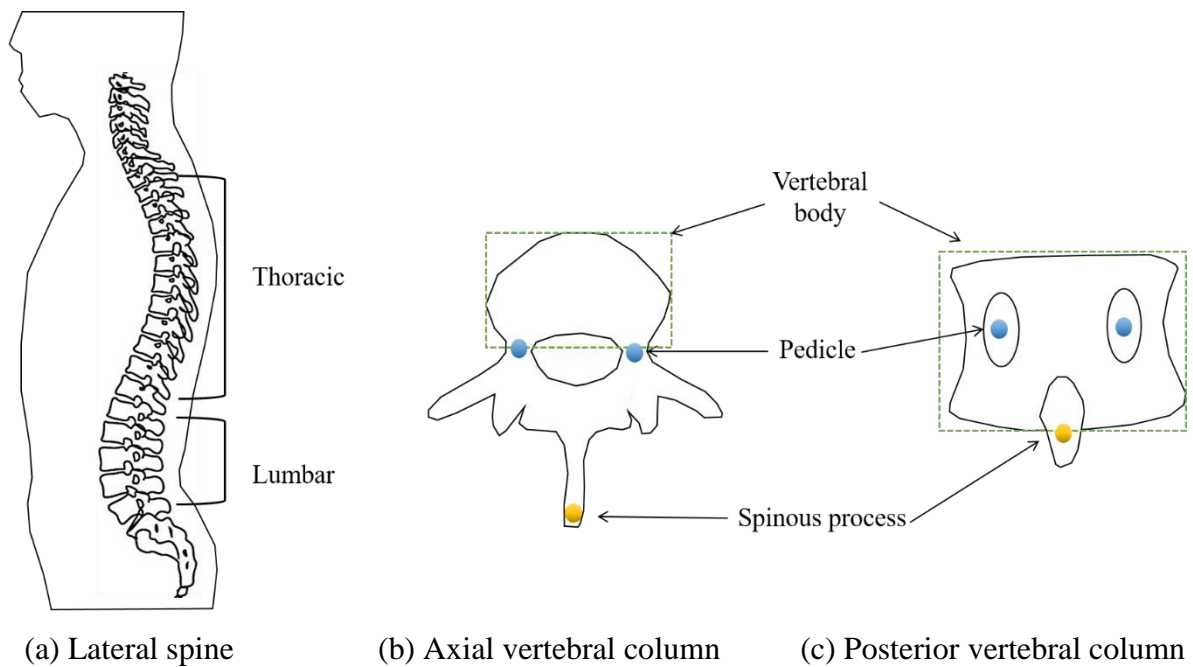


**Figure 1-1** Spinal structure at three different views

(b) and (c) in Figure 1-1 show an axial view and a posterior view of the vertebra respectively. (c) in Figure 1-1 is a simplified figure which is identical to vertebra shown on the X-ray image. In this thesis, spinous process and the vertebral body are used to measure Cobb angle and VR which are the diagnostic criterion of AIS.

## 1.2 Adolescent idiopathic scoliosis

AIS is a spinal disease that develops in teenagers by an unknown cause. AIS is one of structural scoliosis.

There are two types of scoliosis, structural and non-structural. The structural scoliosis, AIS, involves a curve as well as the vertebral rotation, and has the potential to be more serious deformity. In addition, severe deformity in the spine causes serious health problems, i.e., trouble breathing or cardiovascular problems. Because AIS becomes severer deformity if left untreated, teenagers need to get a periodic spinal diagnosis for the AIS diagnosis and the AIS treatment before becoming a serious problem.

On the other hand, the non-structural scoliosis, also known as functional scoliosis, involves only a curve, and develops by temporary causes, like a difference in leg length or a muscle spasm. The non-structural scoliosis is reversible by removing the cause. Therefore, an angle of vertebral rotation (AVR) is a criterion to determine whether AIS or non-structural scoliosis. However, to diagnose with AIS, a threshold of AVR is not defined yet, whereas a threshold of Cobb angle is. It is because AIS had understated as 2D deformity involving only spinal curve until recently. [Placzek et al., 2016, Parvizi, 2010]

The curve larger than  $10^\circ$  is diagnosed with AIS. Table 1-1 shows the treatment option for AIS, including observation, bracing, and surgery. Typically, Observation is recommended to who has the curve smaller than  $25^\circ$ , and Bracing is for the curve smaller than  $50^\circ$ , and surgery is for the curve larger than  $50^\circ$  [Harrington, 1962, Janicki et al., 2007, Placzek et al., 2016 treatment, Weinstein et al., 2008].

**Table 1-1** AIS treatment

Range	Treatment
$10^{\circ} \leq \text{Cobb angle} < 25^{\circ}$	Observation every 4 to 6 months
$25^{\circ} \leq \text{Cobb angle} < 50^{\circ}$	Bracing
$50^{\circ} \leq \text{Cobb angle}$	Surgery

### 1.3 Diagnostic criterion of AIS, Cobb angle and angle of vertebral rotation: their significances and measurements

Cobb angle and the angle of vertebral rotation (AVR,  $\theta$ ) are the criteria for diagnosing AIS involving the lateral bending and the VR. The Cobb angle means the bent angle of abnormal curve in the spine. The Cobb angle is a difference angle between the upper-end and lower-end vertebrae, which are the most tilted vertebrae on the concavity curve as shown in Figure 1-2. The Cobb angle can be more than two in one spine, and the spine is diagnosed as AIS if the maximum Cobb angle is bigger than  $10^{\circ}$  [Cobb, 1948].

AVR means the rotated angle of spinal columns on a transverse plane. There is still no standard method for measuring AVR since AIS has recently started to be understood as a 3D deformity. The AVR is a crucial measure for better insight to the deformity progression. Hence, many methods for measuring the AVR have been reported.

The methods for measuring the AVR can be divided into a 2D method and a 3D method. The 2D method uses a 2D image like an X-ray image, and measures the AVR based on the features, mainly vertebral body and pedicle. The measured AVR is degree, rotation level, or +/- sign. [Lam et al., 2008, Vrtovec et al. 2009, Drerup, 1985]

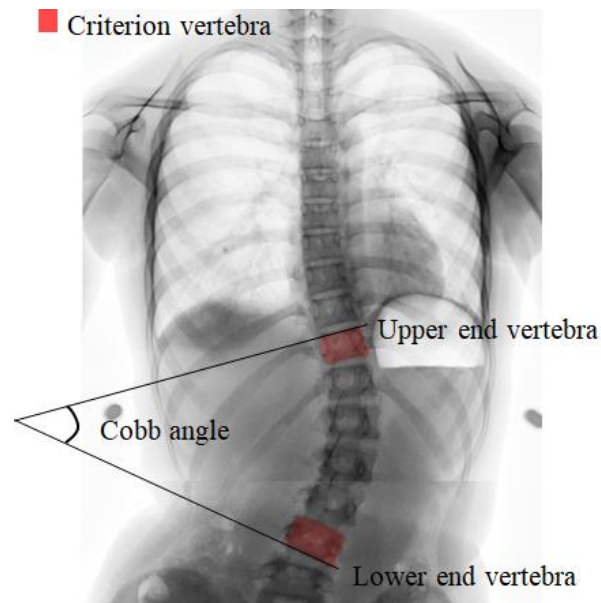


**Figure 1-2** Measurement of Cobb angle

Figure 1-3 shows three 2D methods. Perdriolle's method measured the AVR using a kind of ruler called torsionmeter as shown (a) in Figure 1-3 [Perdriolle et al., 1985]. It considered the most accurate and simplest to use among 2D methods. Cobb's method measured the AVR as an intensity of rotation as shown (b) in Figure 1-3 [Cobb, 1948]. (c) in Figure 1-3 was a method using a rate of features [Monji, unpublished].

The 3D method uses 3D images obtained from CR or MRI, and measures the AVR as a different angle between the reference line and the line connecting vertebral features. The reference line obtains from the coordinate of the used machine.

Figure 1-4 shows three 3D methods. Ho's method using CT measured the AVR based on the vertical line and the bisecting line of the two lines connecting three features on the inner surface of the junction as in Figure 1-4 (a) [Ho, 1993]. In the 3D methods, it estimated the most reliable and clinically useful method [Vrtovec et al. 2009]. Göçen's method measured the AVR based on three features as in Figure 1-4 (b) [Göçen et al., 1999]. Figure 1-4 (c)

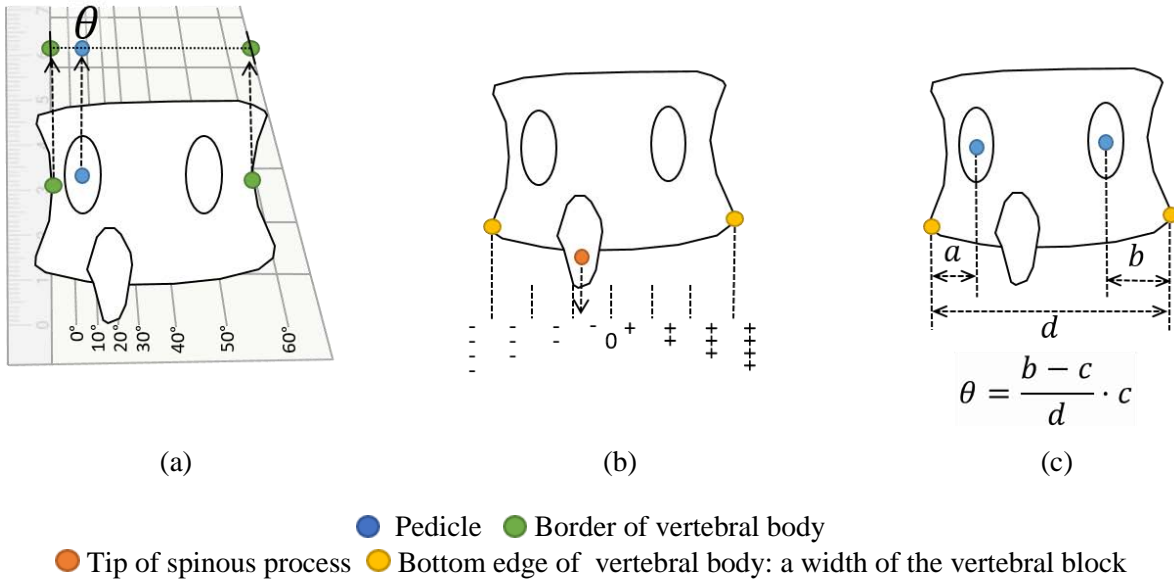


**Figure 1-3** 2D method for measuring AVR ( $\theta$ )

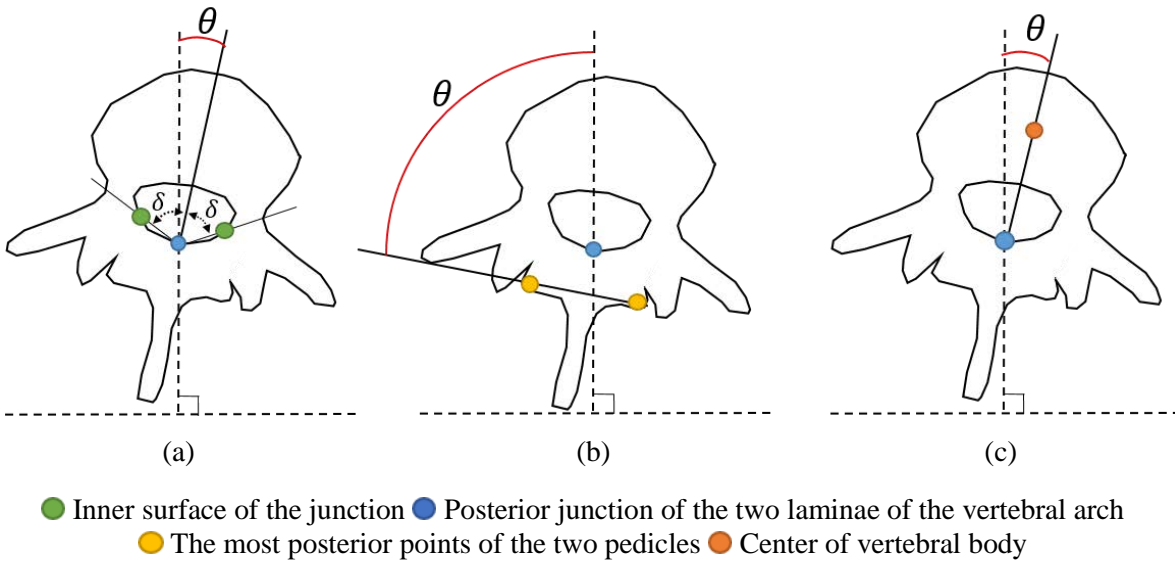


**Figure 1-4** 3D method for measuring AVR ( $\theta$ )

shows Aaro's method measured an angle between the line that connected the point at the posterior junction of the two laminae of the vertebral arch with the center of the vertebral body, and the reference plane [Aaro et al., 1981].

## 1.4 Screening step of AIS

Screening is a strategy that targets the big group in order to identify the possibility of an undiagnosed disease [Screening, 2018]. In Japan, students get the spinal screening during the health checkup, by a Moire method. The Moire method has been used for a long period because it is a cost-effective and suitable method for big groups [Montgomery et al., 1990]. The Moire method captures the Moire image by projecting Moire pattern onto the back of the human body. Using this Moire method, experts take four or five Moire images of one student in one minute.

The steps for spinal screening by Moire method is described in Figure 1-5. A Moire machine captures a Moire image of student [(b) in Figure 1-5]. By the surface metric that obtained by scoring the degree of symmetry on the Moire image, students are classified into two groups, normal or suspected of demonstrating AIS [(c) in Figure 1-5] (The detail of Moire method is described in Section 2.3.5). The group suspected of demonstrating AIS is referred to the hospitals for diagnosing AIS by the additional diagnosis using X-ray [(d) in Figure 1-5]. In this diagnosis step, the diagnosis of AIS is made only by measuring the Cobb angle. Individuals whose diagnosed as mild AIS are recommended to get a periodic monitoring to check the progress of deformity [(e) in Figure 1-5].

During the spinal screening, the use of radiation method except for the diagnosis is reducible and unnecessary. Therefore, there is a possibility that the use of radiation method may be further reduced by nonuse of the radiation for the monitoring, and reduction in the number of individuals suspected of demonstrating AIS.

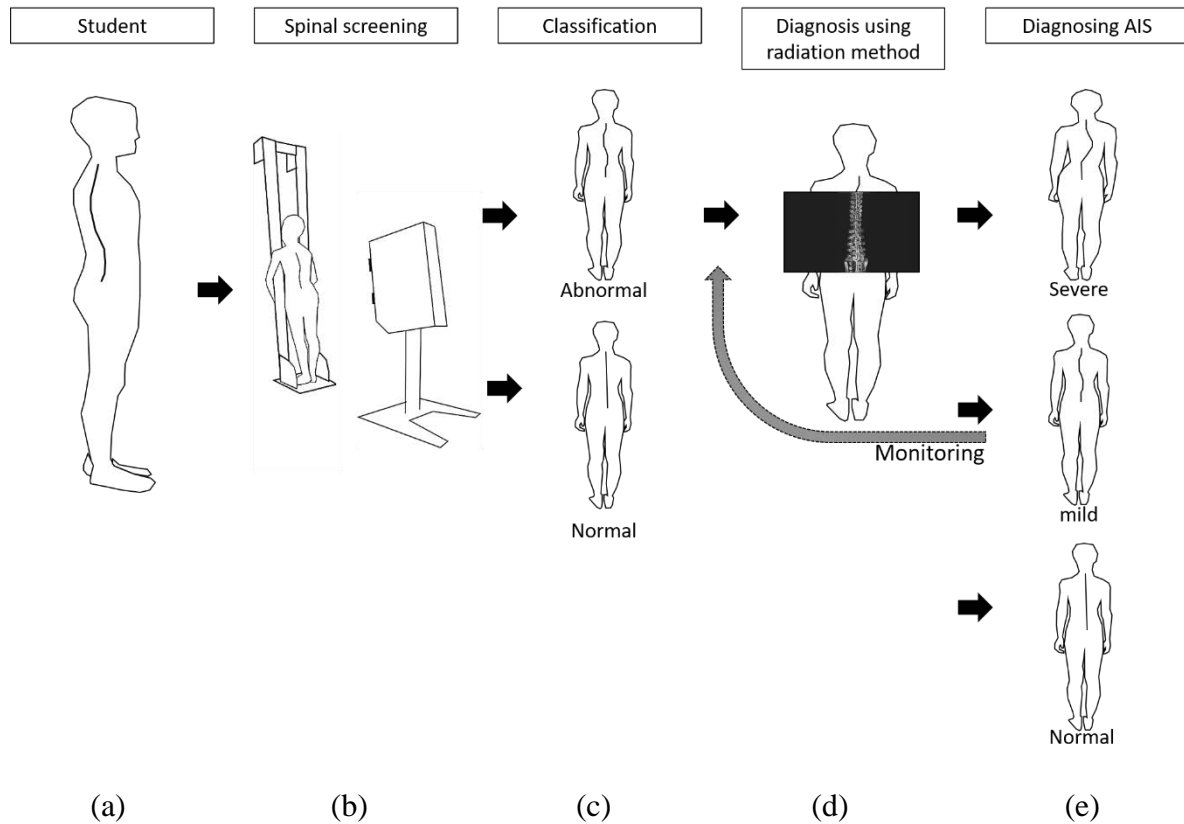


**Figure 1-5** Steps of the spinal screening by a Moire method

### 1.4.1 International state of the spinal screening

We investigated for the international state of the spinal screening whether the spinal screening is implemented, and what kind of method is used for. The summary of it is in Table 1-2. The Moire method is used in Japan and China. Singapore used it, but now Raster stereography is used. Adam's forward bending test is used in almost all over the country. This is because Adam's test does not require any special tool or equipment. In addition, Scoliometer is used for the screening [Altaf et al, 2017, Kuroki, 2017]. Details about the screening methods are introduced in Section 2. Recently, the spine screening has started to be enforced and has been increased by emphasizing of the importance of spine.

**Table 1-2** International state of the spinal screening

Region	School Spinal Screening	Screening method
Japan	-Mandatory by law -Organized at a local	-Moire method -Forward bending test
Canada	- No screening	-
America (NewYork, California, Florida etc.)	- Legislated at 21 states	-Scoliometer -Forward bending test
Hong Kong (China)	-Provided for the student health service	-Moire method -Forward bending test
Singapore	-Routine screening	-Moire method → Raster stereography
Europe	-Not national policy in UK, Poland -National policy in Greece, Italy, Turkey, Bulgaria etc.	-Raster stereography -Forward bending test
Australia	-Supported by medical societies	-Forward bending test

## 1.5 Proposal

We propose a spine estimator that is safe from the risk of radiation, although available to support the assessment of spine like as a result obtained using the radiation method.

Accordingly, our goal is to supply a spine shape with crucial indicators of AIS. To supply these, the Moire image is utilized. It is applicable to minimize the use of radiation method during the diagnostic phase of AIS. The crucial indicate are the Cobb angle and AVR as shown in Figure 1-6.

The key idea why we utilized the Moire image is that the spine shape affects the back surface as shown in Figure 1-7. The concave where is located on the center of back surface corresponds with the spinal shape. This is also the fact used by other conventional optical methods to obtain spinal morphology. Figure 1-8 shows X-ray images and the three different curvatures by the effect of the spinal shape. The spinal curve with harder deformity has more complex pattern. Therefore, the Moire image is used as a descriptor of the back surface. The Moire pattern is a predictable indicator of the spine, and moreover, the morie method has a large amount of accumulated data due to the long period of use.

Figure 1-6 shows the process of the proposed method. From the Moire image, the back area and the spinal positions are estimated by two Convolutional neural networks (CNN). The spinal positions consist of 17 centers of vertebrae bodies and 17 tips of spinous processes including 12 dorsal and 5 lumbar vertebrae. Then, the estimated spine positions are evaluated by two measuring methods, Cobb angle and AVR. The measuring methods are proposed as well.

The spines collected from X-ray or estimated by CNN, consists of only the 2D point data of vertebral features. Therefore, the conventional method for measuring the Cobb angle which uses all spine edges is inapplicable to the estimated results. Moreover, the conventional method for measuring the AVR is also inapplicable because AVR is an axis rotation that requires z-information for the measurement. Given reasons, we propose the measurement methods.

For the Cobb angle, the proposed method only uses 17 x-y points of vertebral center, and measures by calculating inflection points of the spinal curve. For the AVR, the proposed method uses not only 34 x-y points of two features, the vertebral center and the tip of the

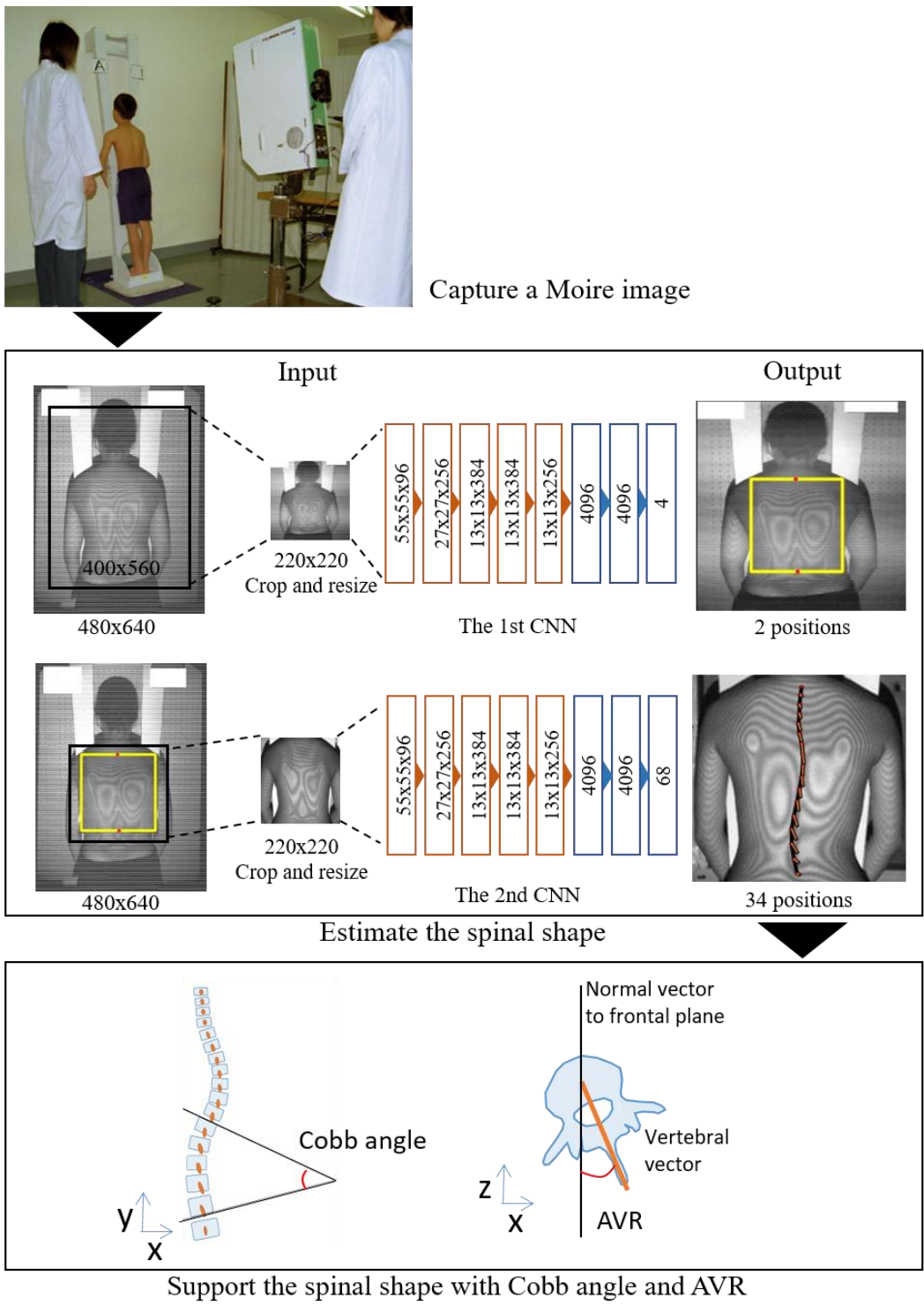


**Figure 1-6** The process of proposed spine estimator

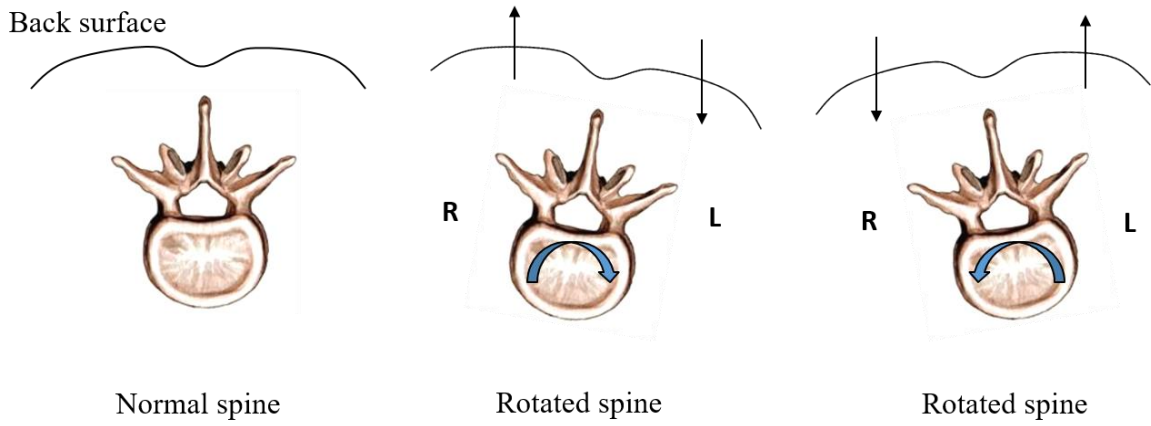


**Figure 1-7** Surface deformations by the rotated spines



**Figure 1-8** Moiré patterns and X-ray images in accordance with each deformity

spinous process, but also 17 lengths between the two features in a transverse plane which is z-information. The proposed method for the AVR measures the angle by calculating the difference between two lines, reference vertical line and the line connecting two features. Here, the lengths are obtained from the spinal model of teenagers and this model is generated from average values collected from CT images.

### 1.5.1 Outline of the thesis

An input of the proposed spine estimator is a Moire image captured by Moire machine. The Moire image is used as the descriptor of the back surface in this thesis. This is because the Moire image has predictable indicators of the spine as well as a large amount of accumulated data. The details of the Moire method and other conventional methods are in Section 2.

The Moire image shows only a surface information. Accordingly, a dataset is generated by merging the Moire image with the spinal positions obtained from X-ray image. A generation method for dataset is explained in Section 3.

We also propose the measuring methods for the Cobb angle and the AVR to obtain AIS indicators from the spine. The method for measuring the Cobb angle measures bent angles of the abnormal spinal curve from 17 centers of vertebral bodies. The method for measuring the VR measures an axial rotation angle (in x-z planes) from 2 points (in x-y planes), and the two points consist of one center of vertebral body and one tip of the spinous process in one vertebra. A general model of spinal size is generated and applied to obtain necessary z information for the VR. The detail descriptions and validations of two measuring method are in Section 4.

CNN is used to estimate the spine from the surface descriptor. Two CNNs are used to estimate the spine. The first CNN estimates a back area from the Moire image. Then, the second CNN estimates both of positions, the 17 centers of the vertebral bodies and the 17 tips of spinous processes, from the back area. A structure of CNN which we used and the

---

result estimated by CNN are described and analyzed in Section 5.

In Section 6, the summary and future works of this thesis are described.

This thesis includes the previous works published in reference [ Choi et al., 2017, Choi et al., unpublished] as follow:

- Introductions of AIS and the Moire method in Section 1 and 2.
- Explanation of related methods including the Moire method, ultrasound methods and radiation methods in Section 2.
- A proposed method for measuring the Cobb angle; Septs to measure Cobb angle and the validation of it in Section 3.
- A proposed method for measuring the AVR; Definition of AVR, modeling, and the validation result in Section 3.
- Result of experiments; The result of estimation by CNN, the analysis result by the measuring method and networks of CNN in Section 5.

### 1.5.2 Contributions of the thesis

Contributions of this thesis are summarized as follow:

- A spine estimator only using Moire image as well as an automatic operation system which does not require any human intervention. The other conventional methods required the human intervention such as a marker attachment to detect a part of a body, or a diagnosis from result data.
- As results, the supply of the spine shape and AIS indicators, the Cobb angle and the AVR; It is the different point from conventional methods which supply the unbalance

---

indicators or classifying whether normal or abnormal. The indicators are critical information for the treatment and assessment of the spine.

- Measurements of the Cobb angle and AVR from 34 points; Whereas other method for measuring the Cobb angle measured based on the edges of vertebrae, the proposed method for measuring the Cobb angle uses the 17 center points of vertebrae. In addition, the proposed method measuring AVR measured an axial rotation angle from 2D points by applying the general model of the spine.

## Chapter 2

# Overview of the proposed system and related works

In Section 2.1, we describe an overview of our method about the detail information of data, the input and output of networks, network structures, and a post-processing to get the Cobb and AVR angles as final results.

In Section 2.2 and 2.3, we introduce two kinds of related works; One is focusing on the automatic measurement of Cobb angle or AVR. Another one is about related methods to the spinal diagnosis or the spinal screening, and with their evaluations. The automatic measurements measured the Cobb angle or the AVR, and mainly used radiation method. The details of these are explained in Section 2.2. There are many kinds of methods for the diagnosis or the screening: radiation methods, optical methods, ultrasound, tools, smartphone applications and Kinect. In addition, there are many indicators to diagnose the spine: imbalance of trunk, symmetric degree, and angle of trunk rotation. The diagnosis/screening methods and their indicators are described in Section 2.3.

## 2.1 Overview of the proposed system

### 2.1.1 Dataset – Moire and X-ray images

We used two kinds of images, Moire and X-ray images, for our system. The Moire image was used to estimate the spinal shape, and the X-ray image was used to make the ground truth of the spine shape. Both images were collected in 2200 pairs through Tokyo health service association and were approved by the IRB.

The Moire images which we collected were taken by two technicians, using a Moire machine (Fujifilm Corp.'s FM40SC II) in dozens of schools. On average it took less 1 minute for one patient. Figure 2.1 shows the environment for a Moire screening; The distance between a patient and a Moire camera was 160 cm, the moire machine and a supporter for a patient were tilted  $10^\circ$ .

In Tokyo health service association, the captured Moire images were evaluated by scoring the symmetry level of Moire pattern, by two medical technologists and then checked by another two medical technologists.

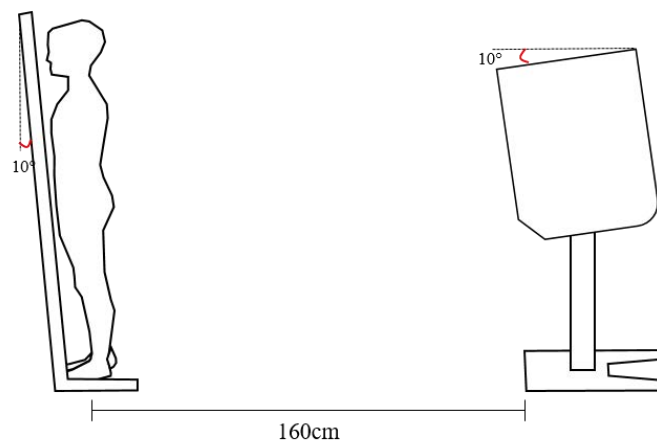
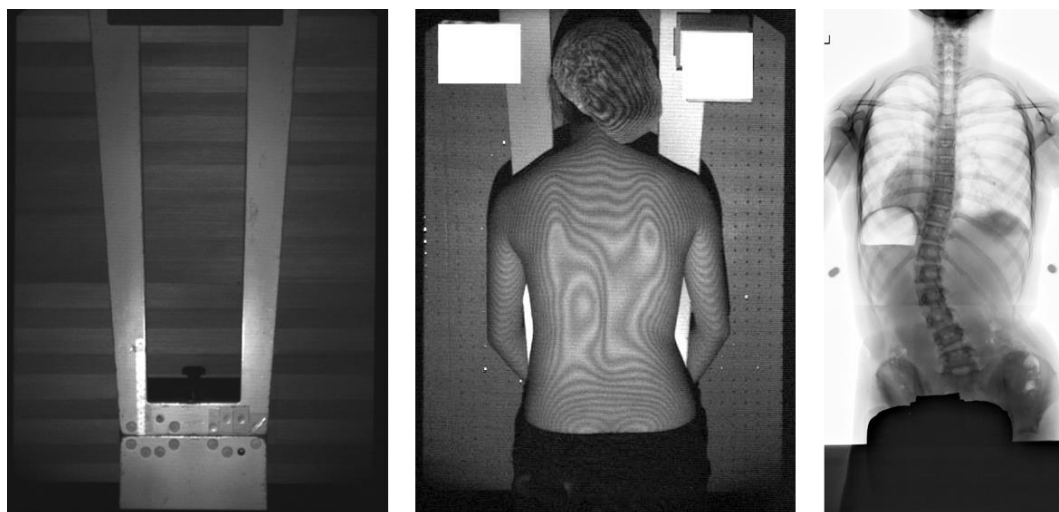


**Figure 2-1** The environment for Moire screening



(a) a Moire image without a patient

(b) a Moire image

(c) a X-ray image

**Figure 2-2** The collected data

Figure 2-2 (a) shows a Moire image of flat background without a patient and the original image of the collected Moire image. Because the Moire machine was tilted  $10^\circ$ , you can see a striped Moire pattern on the Moire image of flat background. Two gratings of the Moire pattern had a pitch of 5mm. The original Moire image [Figure 2-2 (b)] was a grayscale, and the size is  $480 \times 640$  pixels.

The X-ray images were collected from patients who were classified as abnormal by the Moire screening. The X-ray images were taken by a radiological technologist in Tokyo health service association. The used X-ray generators were Canon medical systems Inc.'s KXO-SS/J2 and DST-1000A, and the used X-ray detector was Canon lifecare solutions Inc.'s CXDI-40EC. Unlike the environment of Moire screening, the distance between a patient and a camera of X-ray machine was not fixed. The original image [Figure 2-2 (c)] of X-ray was a grayscale, and the size was not fixed, around  $2200 \times 4400$  pixels.

The collected X-ray images were annotated by 8 doctors, by using a pointing program

which we developed to collect spinal features. The annotated features were four corner of vertebral body, a center of vertebral body, and a tip of spinous process. To merge the Moire and X-ray images for the ground truth, one exterminator annotated two feature points, the neck and waist, on both images. The detail of merging method is described in Section 3.2. The collected Cobb angles of X-ray images used as the ground truths were evaluated by one orthopedic surgeon.

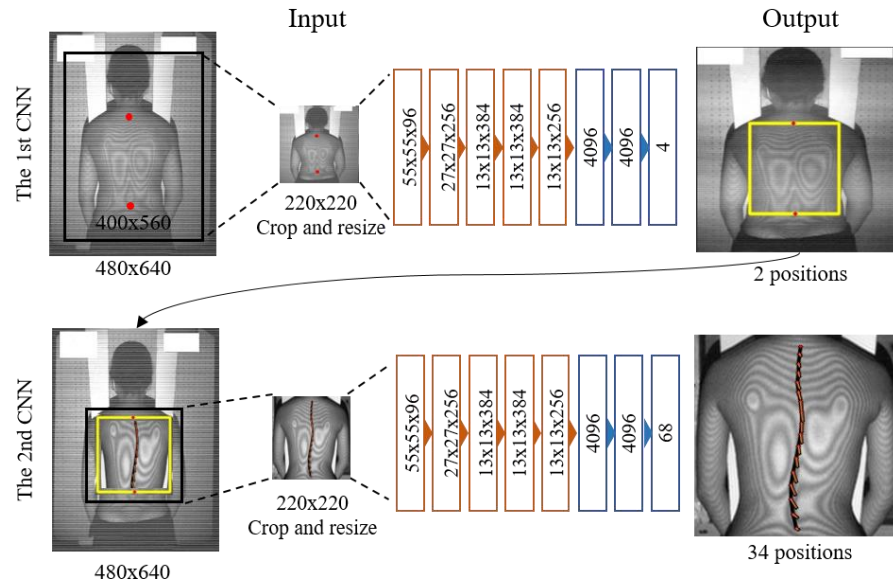
## 2.1.2 Networks

We used CNN to estimate the spinal shape from the Moire image. Figures 2-3 and 2-4 show the input/output and the network structure for the training and the evaluation respectively.

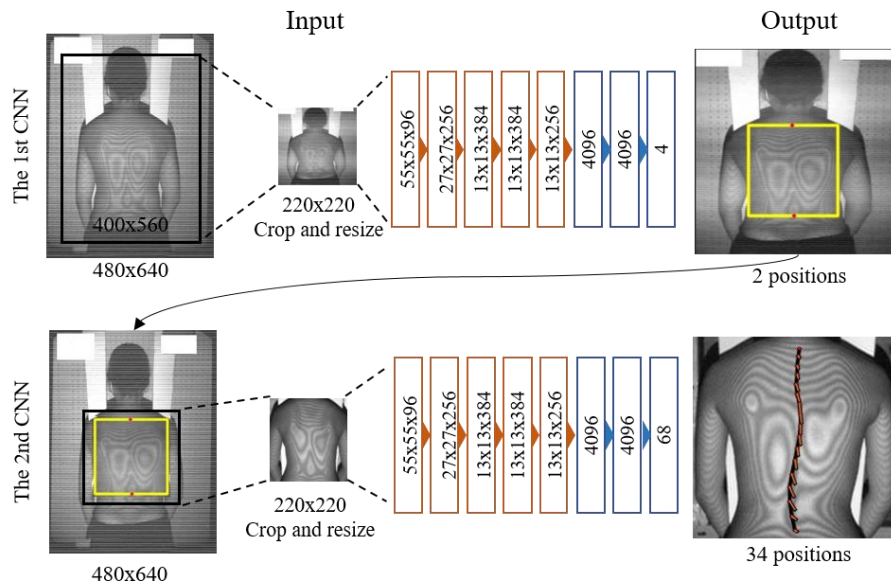
The input and output for the training using CNN are shown in Figure 2-3. The first CNN was trained to extract the back area, and the second CNN trained to estimate the spinal shape from the back area. The inputs were the Moire image with two positions of T1 and L5, and the Moire image with the 34 positions of two features on 17 vertebral bodies for the first and second CNNs respectively. For the first input, the original Moire image (480×640) was cropped to 400×560 at the top-left (40,50). For the second input, the original image was cropped based on the back area. We used 36652 training data which was augmented by rotation (5° clockwise/anticlockwise and mirroring from 1765 data. We used AdaGrad as an optimization method and a learning rate was 0.0005 for the first and second trainings.

Figure 2-4 shows the input and output for the evaluation. The input and output were the Moire image. The Methods for the generation of the input images from the Moire image were identical with the training. The outputs were two positions of T1 and L5, and 34 positions of two features on 17 vertebral bodies for the first and second CNNs respectively. As a test dataset, we used 200 Moire images.

For the training and the evaluation, we used the same network structure of CNN as shown in Figure 2-5. The filter size for a convolution is described as F(width x height, stride,



**Figure 2-3** The Network for training. 36652 data were used for the training.



**Figure 2-4** The Network for evaluation. 200 Moire images were used for the evaluation.

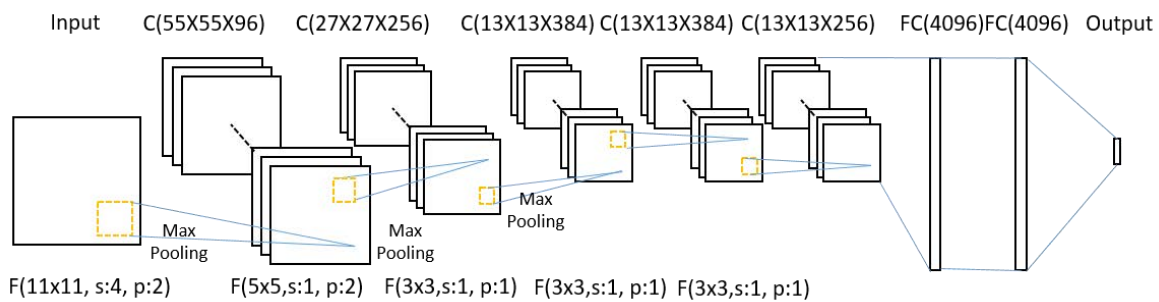


**Figure 2-5** Architecture of CNN

padding). A max pooling was applied  $3 \times 3$  and the stride of it is 2. The details of network structure and the input images are described in Section 5.1.

### 2.1.3 Post-processing

From the estimation result of CNN, we got 34 positions of the spine. Then, based on the estimated result, Cobb and AVR angles were calculated by two methods described in Section 4.1 and Section 4.2., to get indicators of AIS.

## 2.2 Automatic measuring methods of two indicators, Cobb angle and AVR

X-ray images were commonly used to measure the Cobb angle [Sardjono et al., 2013, Zhang et al., 2017, Kundu et al., 2012]. For the AVR, the 3D spine shape by imaging technology was used [Forsberg et al., 2013, Chen et al., 2015, Pomero et al., 2014, Pinheiro et al., 2012]. Methods were reported that used techniques of image processing or the machine learning to get necessary information from radiation image. The automatic measuring methods for Cobb

angle are described in Section. 2.2.1, and the measuring method for AVR is described in Section 2.2.2.

### 2.2.1. The automatic measuring method of Cobb angle

The automatic method for measuring Cobb angle used an X-ray image [Sardjono et al., 2013]. This method defined the left and right edges of the vertebral body by using image-processing. On the edges, particles were located at a regular interval, and the slope values between two neighboring particles were calculated. Finally, based on the two particles having the most extreme slope value, the Cobb angle was calculated.

Another automatic method for measuring Cobb angle was reported that uses machine learning [Zhang et al., 2017]. This method used a deep neural network (DNN) to estimate slope values from an X-ray image, and then, the Cobb angle was measured based on the slope. Figure 2-6 shows the overview of this method. The input of DNN was 50×50 images cropped around each vertebra, and the output was the slope values of each vertebra. The Cobb angle was calculated as the sum of two absolute slopes, which have the maximum absolute values tilting in opposite directions.

### 2.2.2 Automatic measuring method for AVR

Fully automatic method [Forsberg et al., 2013] used CT slice images to measure AVR. From CT slices, the spinal canal and disc were extracted by image-processing using Hounsfield unit (HU) [(a) and (b) in Figure 2-7]. Here, the spinal canal is a spinal line, and a disc is a basement to divide each vertebra.

Using the vertebra size such as the lengths, width and height, the center of vertebral body was obtained based on the fact that the vertebra often is symmetrical [(c) and (d) in Figure 2-

7]. Finally, AVR was measured between the orientation vector connecting the canal and the vertebral center, and the vertebra vector on the spinal line [(e) in Figure 2-7].

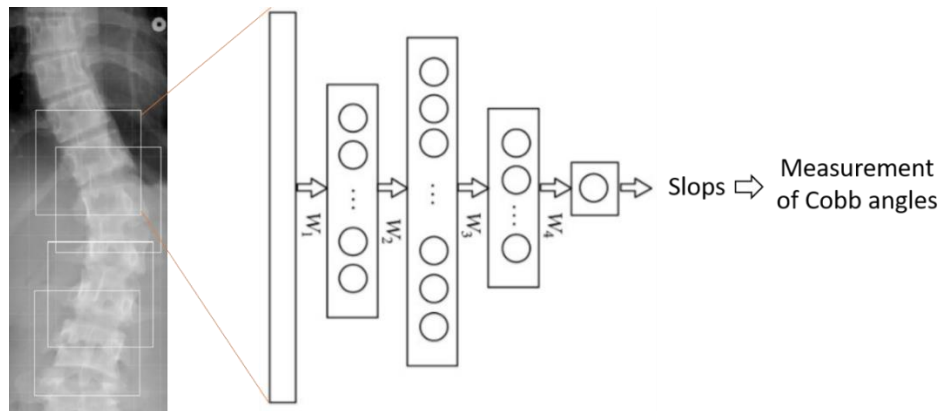


**Figure 2-6** Overview of method using DNN

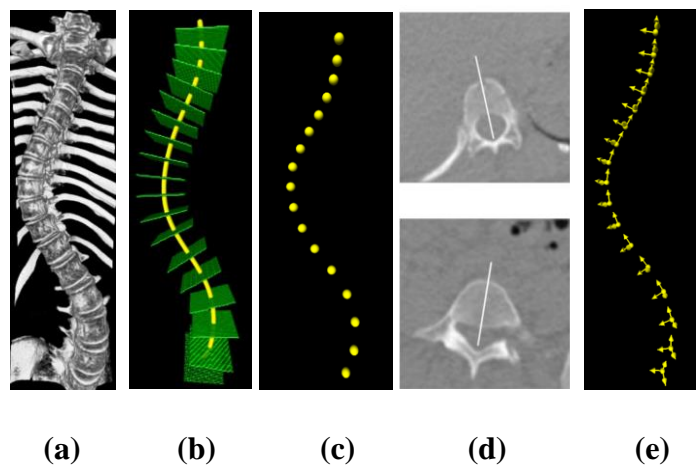


**Figure 2-7** Overview of fully automatic method

---

## 2.3 Spine screening methods and their evaluation

Table 2-1 shows advantages, disadvantages, and evaluation indices of all conventional methods. The detail of the conventional methods, please see from Section 2.2.1 to Section 2.2.10. We compared various spinal screening methods and evaluated the associated indices. The radiation-based methods are highly accurate but are associated with a high risk of radiation exposure. Other methods except the radiation method carry no risk of radiation, but they evaluate the spine using indices that cannot diagnose pathologically and often require manual marking or identification of features.

### 2.3.1 X-ray

The radiograph is the most commonly used 2D method for measuring the Cobb angle. On the radiographic image, the Cobb angle is obtained from the two most tilted vertebrae at both ends of one curve [Cobb, 1948, Cobb angle, 2018]. Many methods exist to measure VR. The Perdriolle method [Perdriolle et al., 1985] is considered the most accurate and simplest to use. It measured the VR based on the position of the pedicle and vertebral body, using a torsionmeter as in Figure 1-3 (a). Because these are manual measurements, observer errors exist. The observer error for the Cobb angle ranges from 3° to 10° [Zhang et al., 2010]. Furthermore, the VR is difficult to measure on radiographic images of poor clarity where feature identification is challenging.

### 2.3.2 CT

CT is a 3D method which can be reconstructed image slides of spine into a 3D spine using imaging techniques. From the 3D spine, the Cobb angle is measured in the coronal plane in the same way as measured on the X-ray. According to the Ho method [Ho et al, 1993] of measuring the VR from the CT, which is considered the most reliable and clinically useful

**Table 2-1** Comparison of the convention screening methods

	Advantage	Disadvantage	Evaluation index
X-ray	-Accurate diagnosis	-Radiation -Manual identification	-Cobb angle -AVR
CT	-Accurate diagnosis	-Radiation -Manual identification	-Cobb angle -AVR
Ultrasound	-Non-radiation	-Manual identification	-Spinous process angle -AVR
Optical method	-Non-radiation	-Require markers	-Surface metrics
Moire method	-Non-radiation	-Manual diagnosis	-Two levels, normal or abnormal
Tools, smartphone application	-Non-radiation -Easy access	-Low accurate	-Angle of trunk rotation
Kinect	-Non-radiation -Automatic method	- Only spinal shape is given for diagnosis	-Spinal shape
Moire method using machine learning	-Non-radiation -Automatic method	- Index is only levels	-Three levels including normal, mild, severe
Adam's forward bend test	-Not required any equipment -Non-radiation	-Manual evaluation	- Imbalance back surface

method, the VR measured based on the vertical line and the bisecting line of the two lines connecting three features on the inner surface of the junction, as in Figure 1-3 (b). The VR measurement from CT data is difficult because it requires identification of the apex of the vertebra from a 3D shape.

### 2.3.3 Ultrasound

Ultrasound does not involve radiation and is a 3D method that is easy to access in hospital settings. Instead of the Cobb angle, the ultrasound measured the spinous process angle (SPA), which is highly correlated to the Cobb angle and uses a line connecting the tips of the spinous process instead of the vertebral body, as shown as Figure 2-8 (b) [Li et al., 2015]. The VR was an angle between the reference horizontal line and the line connecting the two laminae. Figure 2-8 (c) shows detected spinous process with two laminae [Wang et al., 2016]. The detections of the lamina and the spinous process were identified manually on ultrasound images.

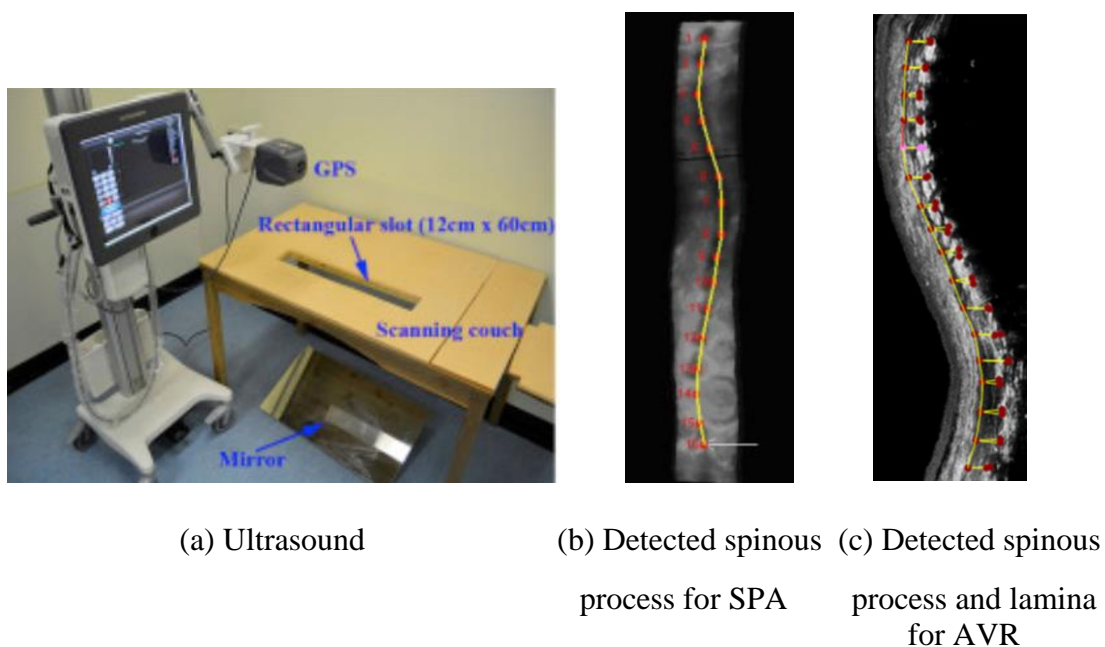


**Figure 2-8** Ultrasound method

### 2.3.4 Optical methods

There are several optical methods: the integrated shape imaging system [Berryman et al. 2008, Weisz et al., 1988, Thometz et al., 1988], the raster stereo photography [Theologis et al., 1997], and Formetric 3D [Drerup, 2014, Drerup et al., 1994, Diers, 2017, Knott et al., 2012, Rankine et al., 2012]. After attaching markers on anatomical landmarks, these techniques measured the back surface using optical technologies such as structured light, and described the spine state based on surface matrices such as shoulder, scapulae, and waist asymmetries, surface rotation, or trunk inclination. As we mentioned, the surface metrics differ from the AIS indices such as the Cobb angle. For additional details on these indices, please refer to reference [Liu et al., 2003, Patias et al., 2010]. The mean difference between X-ray image and the raster stereography was reported 3.21 mm for lateral vertebral deviation and 2.45° for vertebral rotation, and the correlation was very high [Schulte et al., 2008].



**Figure 2-9** Optical method, Fometric 3D

### 2.3.5 Moire method

The Moire method is also an optical method that describes the curvature and depth of back surface, like a contour line. A Moire equipment consists of a Moire machine and a support for the patient as shown in Figure 2-10 (a). The support and Moire machine are tilted by  $10^\circ$ . The Moire machine incorporates a camera and a projector. The Moire pattern of the Moire image shows contour lines representing the depth of the object surface as shown in Figure 2-10 (b). The general Moire pattern on the back is “M”, “O”, and “W” patterns but they are affected by bone, fat, and muscle. The pattern has bilateral symmetry in an upright spine but has a complex pattern if there is a spinal deformity, as in the case of the severe deformity. Hence, the spinal screening using Moire pattern analysis is a practical approach [Smith et al., 2000, Takasaki, 1970].

Using the Moire image, the spine can be classified as either normal or abnormal by the manual scoring of the symmetry level by checking for equal depth. The Moire image shows the shape of the back but can be somewhat ambiguous in its interpretation. Notwithstanding, the Moire method is used due to a cost-effective and simple method [Denton et al., 1992].

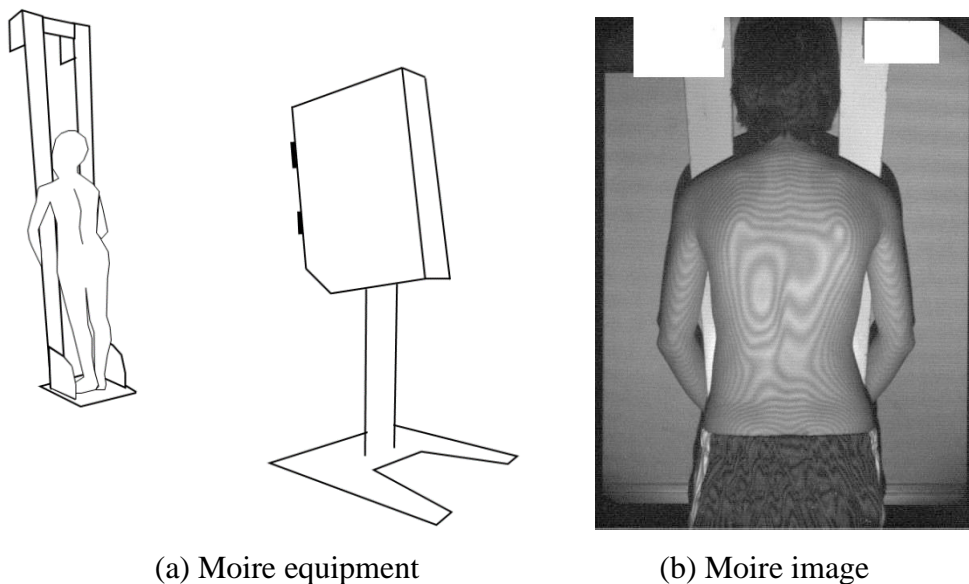


**Figure 2-10** A Moire equipment and a Moire image obtained from the Moire machine

Total 44 subjects were tested by the Moire screening, and the detection rates reported 54% for the curve location, and 100% for kyphosis. [Ruggerone et al., 1986].

### 2.3.6 Machine learning based Moire method

Machine learning based Moire method classified the Moire image to normal or abnormal automatically [Kim et al., 1997, Kim et al., 2000, Ramirez et al., 2006]. The method, first, extracted the middle line of back from a symmetric shape of Moire pattern. Then, four asymmetry degrees were extracted from the Moire pattern, and classified by a neural network (NN) and support vector machines (SVM). As a result, the Moire image was classified into normal or abnormal. This method had the same diagnosis result with the conventional Moire method [Takasaki, 1970] but it operated automatically. A correct classification rate was 88.3%; 80% of normal cases and 95% of abnormal cases were correctly classified [Kim et al., 2000].

### 2.3.7 Moire method using an image processing

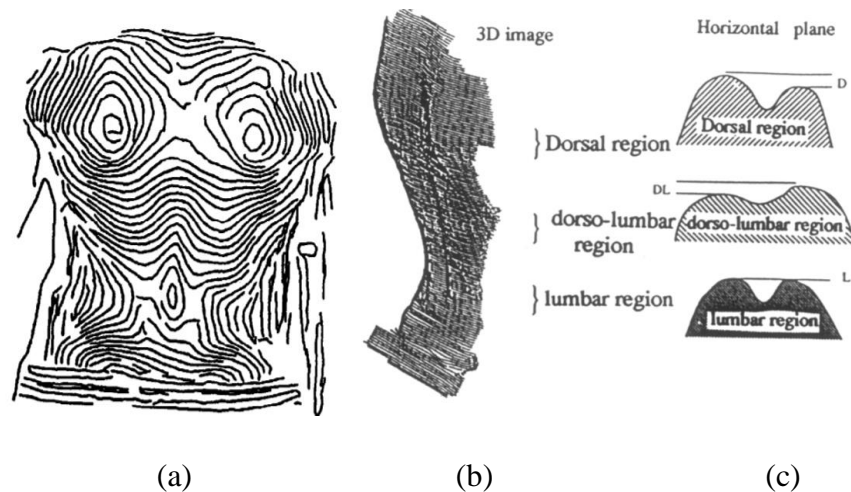


**Figure 2-11** A Moire method using an image processing

The Moire image also used for the automatic diagnose by image processing as well [Batouche et al., 1996]. The Moire pattern extracted as shown in Figure 2-11 (a) and then the extracted pattern was reconstructed to a 3D image as shown in Figure 2-11 (b). The reconstructed image was used to diagnose the spine as 6 conditions, a normal, a simple curvature scoliosis, a double curvature scoliosis, hyperkyphosis, hyperlordosis, or planar back. The spine was diagnosed based on the 3 different depths on a dorsal region, a dorso-lumbar region, and a lumbar region as shown in Figure 2-11 (c).

### 2.3.8 Kinect

Kinect is a method that uses an RGB-D sensor for automatically estimating anatomical landmarks and spinal curve [Castro at al., 2017, Tanee at al.,2017, Ko]. This automated method for estimating landmarks replaces manual marking required during the use of optical methods [Bonnet et al., 2016]. Kinect shows promise as a screening system that uses sensors instead of optical technology. Another research using Kinect [Antal, 2015] generated a virtual Moire image based on the depth image, and evaluated the spine.

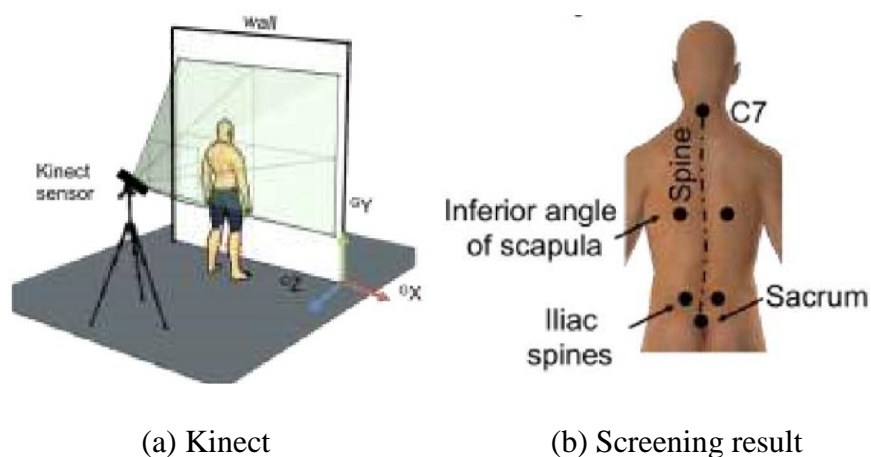


**Figure 2-12** Screening of AIS using Kinect

### 2.3.9 Adam's forward bend test

Adam's forward bend test does not require any requirement, and you just need to bend your back toward. This is effective in a scoliosis detection due to a rib hump or spine asymmetry caused by scoliosis [Adams, 2018].

Adam's pose for the forward bend test is a standing posture with feet and knees together, and bending toward from the waist until the back with the palm facing each other. To detect scoliosis, spinal and scapular asymmetry or unbalance shoulders and hips are checked. When abnormal spine, the back surface or spine look unbalanced like (b) in Figure 2-13 [Altaf, 2013]. Adam's forward bend test was rated as more sensitive than Scoliometer (see Section 2.3.10) which rated having low accuracy [Côté et al., 1998].

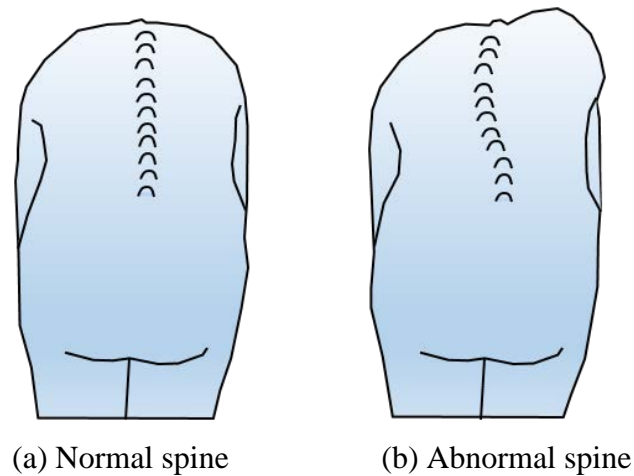


**Figure 2-13** Adam's forward bend test

### 2.3.10 Tool and smartphone application

Additional smartphone applications [Franko et al., 2012] which use a built-in gyro sensor, such as Scoliometer and Scolioscreen exist. Such applications are easily accessed, requiring only downloading of their application. Moreover, they are easy to operate, requiring the user

to only drag the phone (supported by the thumbs) along the spinal curve as shown in Figure 2-14. These applications can measure the angle of trunk rotation (ATR) in Adams test position, similar to Scoliometer [Amendt et al., 1990], which is a small tool for measuring ATR. These methods do not require specific training; however, its accuracy is low because the ATR can be measured differently depending on the position of the thumbs or the phone. Scoliometer was reported that it is not sufficient to use as the decisions for the treatment because of low correlation coefficients around 0.4 (from 0.32 to 0.54) between ATR and the Cobb/AVR angles.

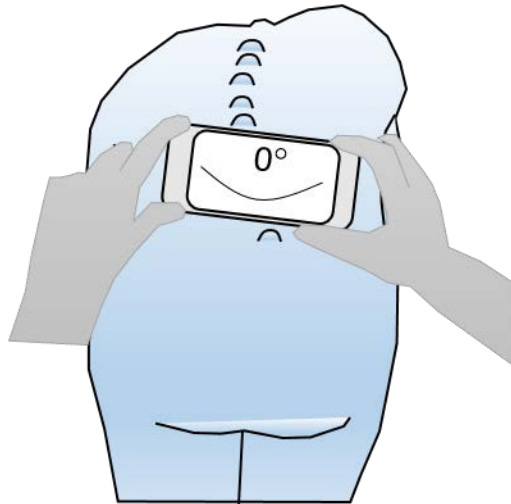


**Figure 2-14** Smartphone application



## Chapter 3

# Generation methods for a dataset

We need to prepare a dataset for the training and estimation of the spine shape. Based on the method for generating a dataset, the result can have high accuracy or low accuracy. In chapter 3, we examine using several datasets to identify the best method for generating the dataset. Moreover, we examine which feature point is better to be estimated by CNN.

Here, we explain what kind of data we collected for the dataset, and how to generate the dataset from the collected data. In Section 3.4, there are conclusions for the optimal dataset.

### 3.1 Feature collection for the dataset

To estimate the spinal positions from the Moire image, numerous Moire images with spine information are needed as a dataset for machine learning. However, the spinal positions cannot be detected if the Moire image is used alone. Therefore, we collected two types of

data from the same patient, a Moire image and a radiographic image that includes manually annotated spinal features.

Figure 3-1 shows the features including a center and four corners of vertebral body, the tip of spinous process and two pedicles. The center of the vertebral body was collected automatically from the four corner of the vertebral body. The collected spine included twelve thoracic vertebra blocks and five lumbar vertebra blocks.

The center of vertebral body was used to measure Cobb angle and two features, the center of vertebral body and tip of spinous process, were used to measure AVR. The pedicles were collected as a feature which is usable instead of the tip of spinous process when measuring AVR. Resultantly, it was not used for measuring AVR. The reason and detail about why we collected it are explained in Section 3.3. The collected data consisted of spines of teenagers from 10 to 16 years old, having Cobb angles from  $0^{\circ}$  to  $55^{\circ}$ .

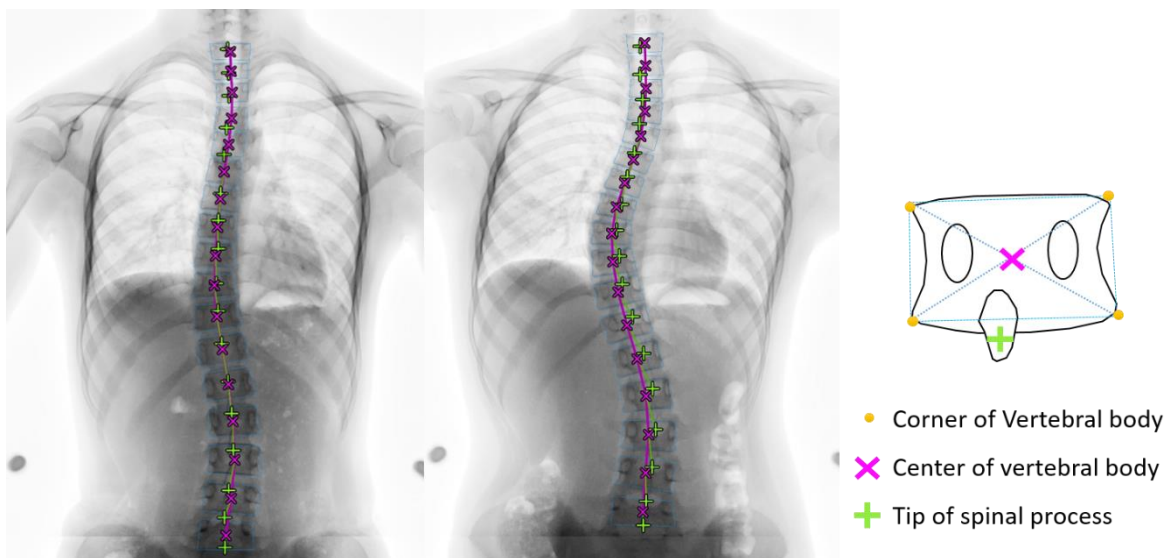


**Figure 3-1** The annotated features on the X-ray image

---

## 3.2 Dataset generation

We collected two kinds of data, the Moire image and the several features of the spine from the X-ray image. In this Section, we explain that what is a difficulty to merge the two data, and how to merge the two data accurately to generate the dataset.

### 3.2.1 Mergence method of two data

To merge the two data, i.e., the Moire image and the spine information on the X-ray, the X-ray should be overlap with the Moire image based on the silhouettes of the body by scaling and translation (Figure 3-2) because there was no anatomical landmark in common on both the Moire image and X-ray. In this case, merging the two images can be problems by the differences of the poses on the images, and of viewpoints of two cameras. In Figure 3-3, Two images are poorly fitted because of the differences of the camera's viewpoints, and of the patient's poses.

To merge the two images accurately, they should be calibrated to have the same coordinate system and one pose should be transformed into the other pose. This is difficult because of not only its complexity but also the limited information of the camera viewpoints in the data, which was collected under dozens of different environments. For more accurate fitting using a simpler procedure, we applied a perspective projection under the hypothesis that the surfaces of the back on the Moire and X-ray images are an identical plane viewed from different viewpoints.

Perspective projection [Dubrofsky, 2009, Carlbom et al., 1978] represents an object as seen from the viewpoint of the observer. It is used for mapping 3D points onto a 2D plane in the field of computer graphics. This projection is expressible as the relationship of the same object from different viewpoints. If locations of the features on the 2D plane from two different viewpoints are known, a shape/image at one viewpoint can be transformed to that

at another viewpoint. Thus, perspective projection is able to generate a more fitted result using feature points than simple translation and scaling to merge different viewpoints and small movements of the subject between images.

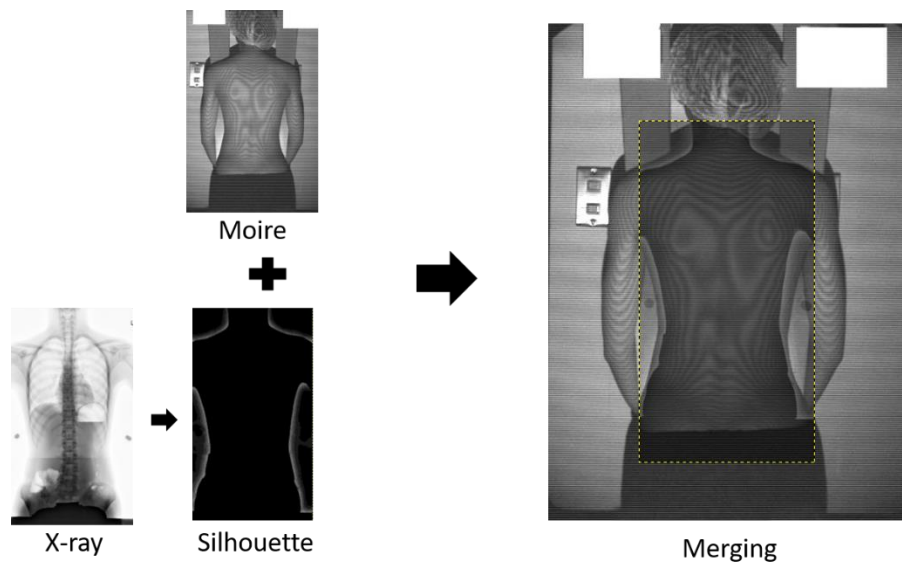


**Figure 3-2** Merging process based on the silhouette

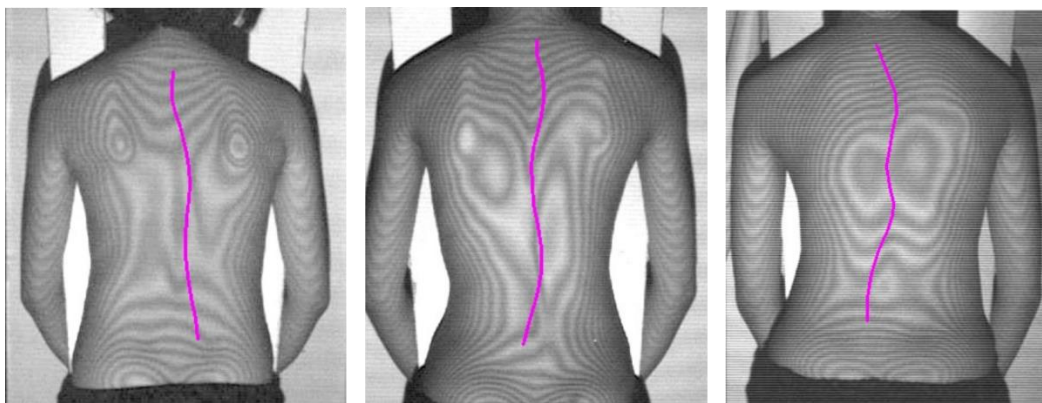
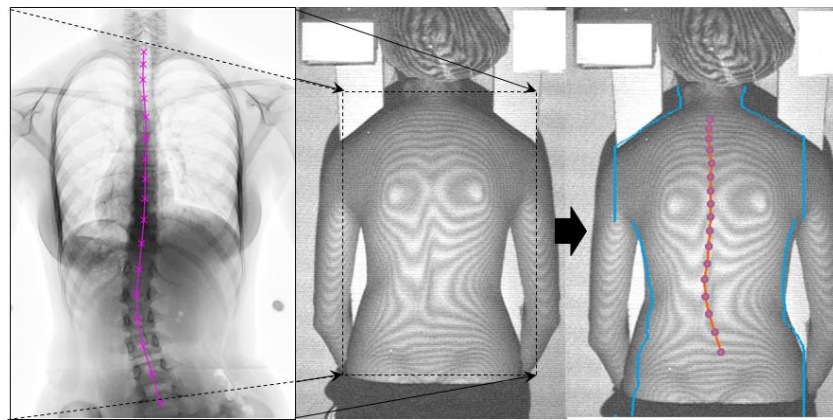
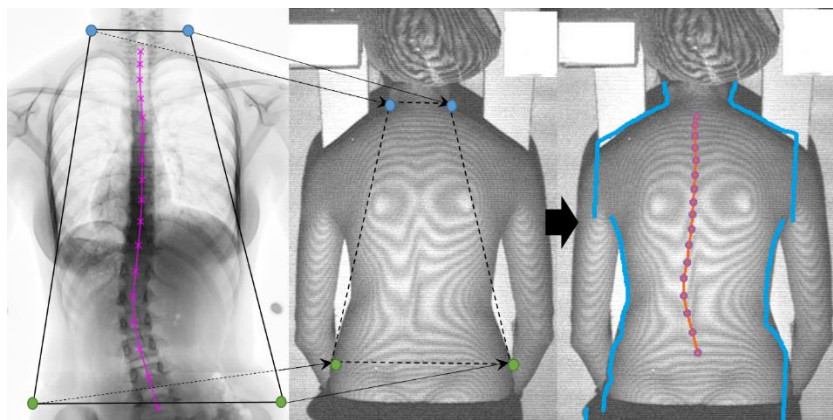


**Figure 3-3** Poorly fitted spine shape



(a) Merged by translation and resize



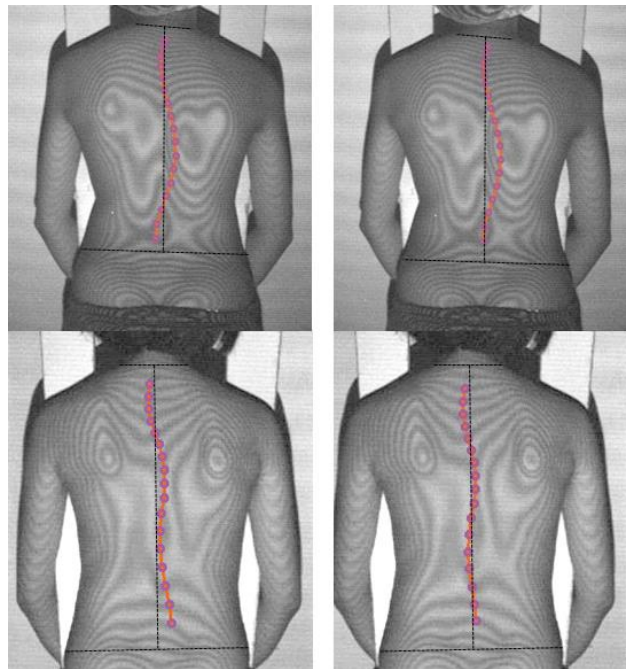
(b) Merged by perspective transform.

● Neck points, ● Waist or pelvis points

**Figure 3-4** Methods for merging two images

The algorithm to merge the two images used strong curve features on the neck, waist, and pelvis. Using these features on the corresponding parts in both images, the reference planes for projection was generated and combined by perspective projection for merging. The strong features consist of four positions: both sides of the neck and both sides of the waist, or both sides of the neck and both sides of the pelvis. After the four features on both images had been

located manually, the plane in the X-ray was projected to the other plane in the Moire image, as shown in Figure 3-5 (b). Typically, the spine is located at the centers of the neck and pelvis. In (a) and (b) in Figure 3-4, both ends of the vertebrae on the spine are located at the center of the neck and pelvis on the image merged by perspective projection but not on the image merged by translation and scaling. The formulae using four feature points are shown below (1) and (2). In (1), neck points are  $(x_1, y_1), (x_2, y_2)$ , and waist or pelvis points are  $(x_3, y_3), (x_4, y_4)$ .  $(x', y')$  is a point on the Moire image and  $(x, y)$  is a point on the X-ray. First, a homography matrix was created by (1).  $h_{33}$  of the homography was 1. Then, the transformed image was created by (2). In (2),  $(x_l, y_l)$  is input position and  $(x_o, y_o)$  is output position.



(a) Results merged by translation and resize      (b) Results merged by perspective transform

**Figure 3-5** Merged results

$$\begin{bmatrix} x_1 & y_1 & 1 & 0 & 0 & 0 & -x_1x'_1 & -y_1y'_1 \\ 0 & 0 & 0 & x_1 & y_1 & 1 & -x_1y'_1 & -y_1y'_1 \\ x_2 & y_2 & 1 & 0 & 0 & 0 & -x_2x'_2 & -y_2y'_2 \\ 0 & 0 & 0 & x_2 & y_2 & 1 & -x_2y'_2 & -y_2y'_2 \\ x_3 & y_3 & 1 & 0 & 0 & 0 & -x_3x'_3 & -y_3y'_3 \\ 0 & 0 & 0 & x_3 & y_3 & 1 & -x_3y'_3 & -y_3y'_3 \\ x_4 & y_4 & 1 & 0 & 0 & 0 & -x_4x'_4 & -y_4y'_4 \\ 0 & 0 & 0 & x_4 & y_4 & 1 & -x_4y'_4 & -y_4y'_4 \end{bmatrix} \begin{bmatrix} h_{11} \\ h_{12} \\ h_{13} \\ h_{21} \\ h_{22} \\ h_{23} \\ h_{31} \\ h_{32} \end{bmatrix} = \begin{bmatrix} x'_1 \\ y'_1 \\ x'_2 \\ y'_2 \\ x'_3 \\ y'_3 \\ x'_4 \\ y'_4 \end{bmatrix} \quad (1)$$

$$\begin{aligned} w &= x_I h_{31} + y_I h_{32} + h_{33} \\ x_o &= x_I h_{11} + y_I h_{12} + h_{13}/w \\ y_o &= x_I h_{21} + y_I h_{22} + h_{23}/w \end{aligned} \quad (2)$$

### 3.2.2 Evaluation of results used the different mergence methods

**Table 3-1** Error of the datasets generated by different methods

	MAE	SD
Translated dataset	4.7°	3.5°
Projected dataset	4.3°	3.3°

To ascertain if the perspective projection is an effective method, we compared the estimation results using two datasets applied for each method, the scaling/translation (non-perspective projection) and the perspective projection.

The numbers of the training data and the test data were (800,75) for the translated dataset

---

and (899,80) for the projected dataset. These datasets are for the category of teenagers, 10–16 years old having ( $0 < \text{Cobb angle} \leq 50$ ). The training process was equal to the description in Section 5.1.

As shown in Table 3-1, the mean absolute error (MAE) and standard deviation (SD) were  $4.7^\circ$  and  $3.5^\circ$  in the translated dataset and  $4.3^\circ$  and  $3.3^\circ$  in the projected dataset. The MAE of the projected dataset has a small error. Therefore, the dataset applied the perspective projection has high accuracy.

### 3.3 Dataset component

We needed to estimate one feature for Cobb angle and two features for AVR. Both methods needed the center of the vertebral body, and the AVR needed one more feature, the spinous process or the pedicle which are shown on the X-ray image more clearly than other features. In this Section, we compare the results based on the different components of datasets to know which one has better performance. In addition, we compare the results used two different features, the spinous process or the pedicle, to know which one has a more accurate result for the AVR.

#### 3.3.1 Component method for a dataset

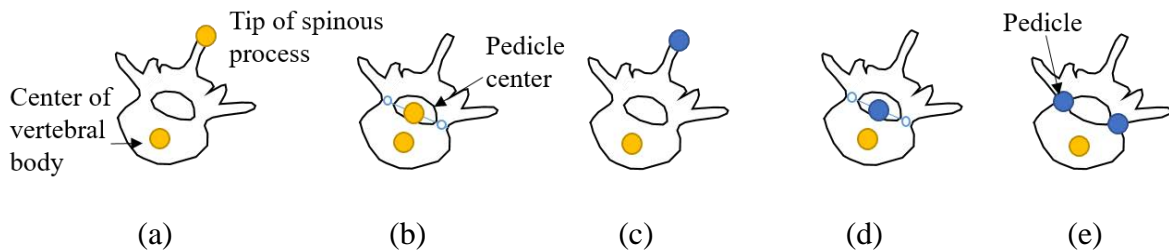
Figure 3-6 shows five different datasets that we generated. In Figure 3-6, (a) consist of the center of the vertebral body and the tip of the spinous process, and (b) consist of the center of the vertebral body and the center of two pedicles. (a) and (b) were trained two features together, therefore the output of CNN were 34 points. (c), (d), and (e) consist of the center of vertebral body and the tip of spinous process, and the center of the vertebral body and the center of the two pedicles, and the center of the vertebral body and the two pedicles respectively. (c) and (d) were trained two kinds of features separately, therefore the output of

CNN was 17 points for each. (e) was trained the center of vertebral body alone, and two pedicles together, thus, the output for the center of vertebral body was 17 points, and output for the pedicles was 34 points.

### 3.3.2 Evaluation of results used the different component of datasets

Table 3-2 shows the result of estimation by CNN according to the datasets and it is visualized in Figure 3-7. In Table 3-2, MAE of AVR and MAE of curve angle were measured using the measurement methods for AVR and Cobb angle which are described in Section 4.

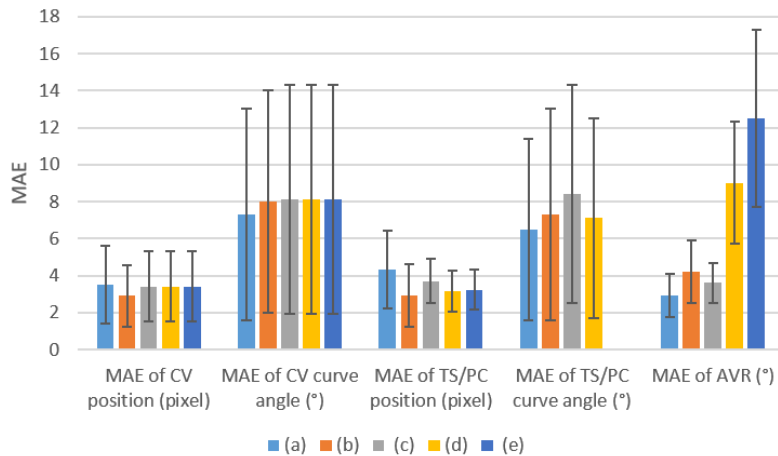
When compared MAEs of AVR in (a) and (b), or (c) and (d), the tip of the spinous process was a better feature to estimate, which have higher accuracy than the center of the pedicle. Synthetically, the training two features together, which are the center of the vertebral body with the tip of the spinal process, shown the best performance.

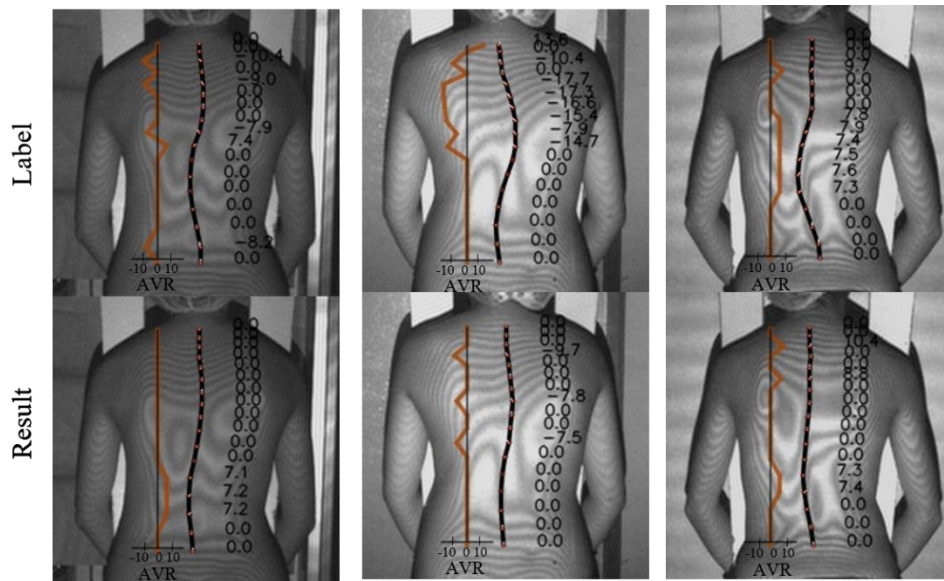


**Figure 3-6** The used features in five datasets. (a, b) are trained two kinds of features together in one CNN, and (c-e) are trained each feature separately in two CNNs. In a dataset, the features marked in the same color means that the features are trained in same CNN.

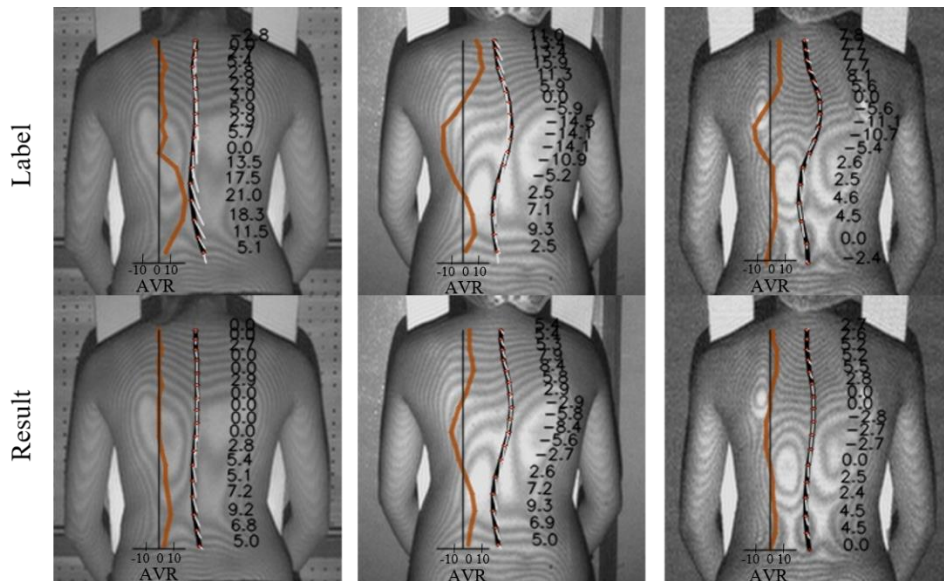
**Table 3-2** the estimation results by CNN according to the datasets

	Dataset	Name of feature	MAE of position (unit : pixel)	MAE of max curve angle	MAE of AVR
Train Together	(a)	Center of vertebral body	3.48	7.3°	2.9° ± 1.16°
		Tip of spinous process	4.3	6.5°	
	(b)	Center of vertebral body	2.9	8.0°	4.2° ± 1.7°
		Pedicle center	2.9	7.3°	
Train Separately	(c)	Center of vertebral body	3.4	8.1°	3.6° ± 1.1°
		Tip of spinous process	3.7	8.4°	
	(d)	Center of vertebral body	3.4	8.1°	9.0° ± 3.3°
		Pedicle center	3.17	7.1°	
	(e)	Center of vertebral body	3.4	8.1°	12.5° ± 4.8°
		Pedicles	3.23	-	

**Figure 3-7** Comparison among MAEs of each dataset. CV is a center of the vertebral body, TS is a tip of the spinous process, and PC is a pedicle center.



(a) Estimation result of the center of vertebral body with the center of the pedicles



(b) Estimation result of the center of vertebral body with the tip of the spinous process

**Figure 3-8** Estimation results. The black curves at the middle of Moiré images are spinal curves connecting the 17 centers of the vertebral bodies. The white lines are lines connecting two features of each vertebra, the center of the vertebral body and the center of the pedicles,

---

or the center of the vertebral body and the tip of the spinous process. The numbers next to the spinal curve mean AVR of each vertebra, and the orange lines are AVR graph.

Figure 3-8 shows the estimation results of the datasets which correspond to Figure 3-6 (a) and Figure 3-6 (b). In Figure 3-8 (a), the white lines are almost not shown since the center of the pedicles estimated where is near the center of the vertebral body. On the other hand, on label image and result image in Figure 3-8 (b), the directions of white line are similar to each other, and the curves of AVR graph have a similar shape to each other. Therefore, we decided to estimate the spinous process for the AVR, not the pedicle.

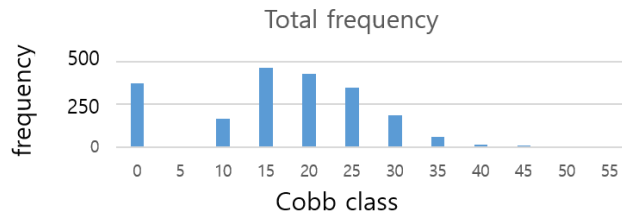
### 3.3.3 Component ratio of patients in the dataset

In the beginning, we made a test dataset by picking up randomly from the collected dataset, and made a training dataset using rest of the collected dataset. However, the result of these datasets was not good, especially in cases of severe deformity. In addition, the Cobb angles of the results tended to have smaller angles than the Cobb angles measured by doctors. In this Section, we compare two datasets. One is generated to be had a balance on the deformity levels, and another one is generated by picking up randomly.

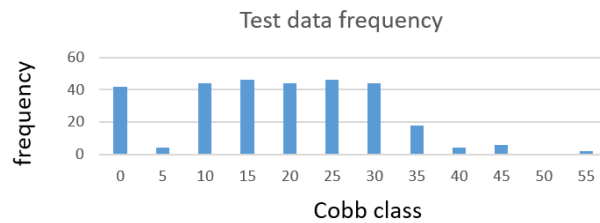
Table 3-3 shows the frequency of dataset. We generated two datasets from the 2061 collected data. From the collected data, the training dataset with the balance had 31% of normal, 32% of mild deformity, and 36% of severe deformity like Figure 3-9. Figure 3-9 shows the frequency graphs. Totally, the dataset with the balance included 1750 data. While the dataset without the balance included all of collected data. The training dataset and test dataset were generated by picked it up randomly like other general datasets for CNN.

**Table 3-3** Frequency of dataset

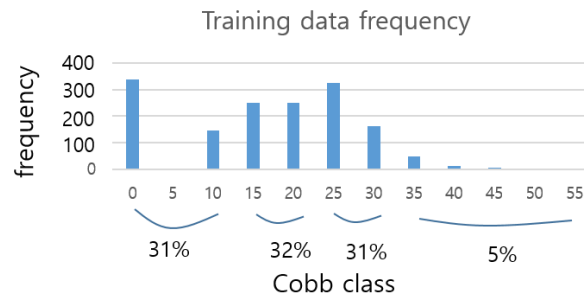
Class based on Cobb angle (CA)	Total Frequency	Dataset with a balance		Dataset picked up randomly	
		Test data frequency	Train data frequency	Test data frequency	Train data frequency
0 (CA=0)	372	21	337	19	180
5 (0<CA≤5)	7	2	5	2	5
10 (5<CA≤10)	168	22	146	12	156
15 (10<CA≤15)	464	23	250	41	221
20 (15<CA≤20)	428	22	250	38	190
25 (20<CA≤25)	346	23	323	24	122
30 (24<CA≤30)	186	22	164	8	178
35 (30<CA≤35)	160	9	51	4	156
40 (35<CA≤40)	16	2	14	0	16
45 (40<CA≤45)	11	3	8	2	9
50 (45<CA≤50)	1	0	1	0	1
55 (50<CA≤55)	2	1	1	0	2
total	2061	150	1600	150	1236



(a) Frequency of the collected data



(b) Frequency of test data considering the balance



(c) Frequency of training data considering the balance

**Figure 3-9** Graphs of frequencies. Cobb class means a unit which is divided Cobb angles, and includes Cobb angles smaller than the number of Cobb class.

### 3.3.4 Evaluation of component ratio of patients in a dataset

Figure 3-10 shows the worst estimation results of two datasets, one with the balance and another one without the balance. In both datasets, the estimated results were not good, but if you look at the results of the calculated Cobb angle, the dataset with the balance is better.

Table 3-4 shows the MAE of Cobb angle of each dataset. In comparison, the dataset with the balance had  $5.8^\circ$  which was smaller than  $9.8^\circ$  of the dataset without the balance.

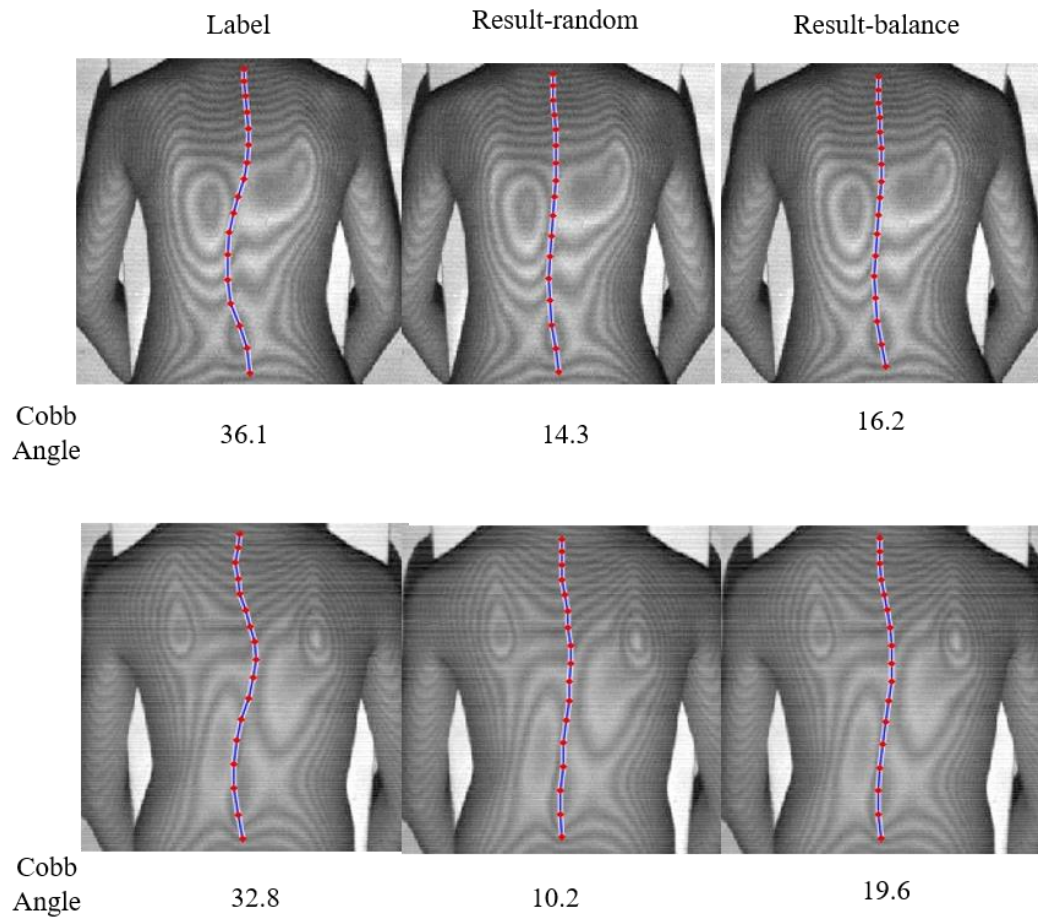


**Figure 3-10** Results trained using two datasets generated with the balance, and generated randomly

**Table 3-4** Results of two datasets

	MAE of Cobb angle	SD
Dataset with the balance	8.7°	6.5°
Dataset picked up randomly	9.9°	6.7°

### 3.4 Conclusion of the dataset

We compared the datasets generated by different methods, the datasets having different components, and the datasets having different component ratios of the deformities respectively. Consequentially, our dataset was generated using perspective projection, and had a balance on deformity levels, normal, mild deformity, and severe deformity. In addition, the dataset for the Cobb angle included the center of the vertebral body, and the dataset for AVR included the center of the body and the tip of the spinous process.

## Chapter 4

# Measurement methods of Cobb angle and of AVR

Measurements of two indicators, Cobb angles and AVR, are necessary to diagnose AIS pathologically. In this thesis, we propose methods of measuring the Cobb angle and the AVR from the feature points collected from X-ray images. The measurement methods are also applied for the estimated results to measure these two indicators of the estimated result by CNN. This chapter describes the details and validations of both methods.

### 4.1 Proposed Method for measuring Cobb angle

To measure Cobb angles from only center points of vertebral bodies, we proposed a measuring method and described detail here. It is a different point from other conventional methods [Cobb, 1948, Sardjono et al., 2013] using the shape of vertebral body.

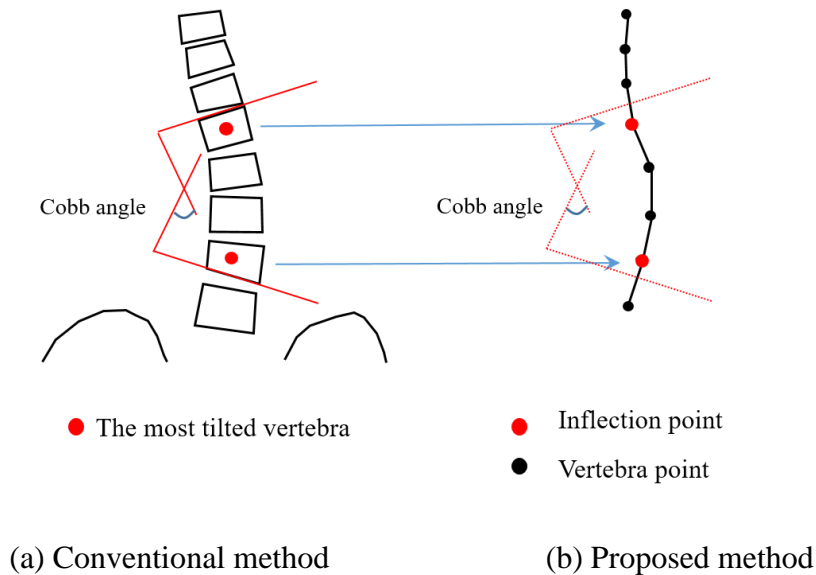


**Figure 4-1** Comparison the conventional method with the conventional method

The Cobb angle is an angle between the most tilted vertebrae where are located at both ends in a single concave curve of the spinal curve as shown in Figure 4-1 (a). The Cobb angle is measured based on two lines, one is parallel to the upper surface of upper-end vertebra and another one is the parallel to the lower surface of lower-end vertebra [Cobb, 2018].

The most tilted vertebra is the point where the curvature of curve changes, such as an inflection point on the spinal curve connecting vertebra points. Therefore, to measure the Cobb angle, we found the inflection points from the spinal curve, and measured the angles between vertical lines to the curve at the two adjacent inflection points. When measured it, we obtained the vertical line where is the mid-point between upper-end vertebra and vertebra above it or lower-end vertebra and vertebra below it, as shown in Figure 4-1 (b). The proposed method of measuring Cobb angle proceeds as flow:

- 1) Fit a curve to the 17 positions using cubic B-spline.

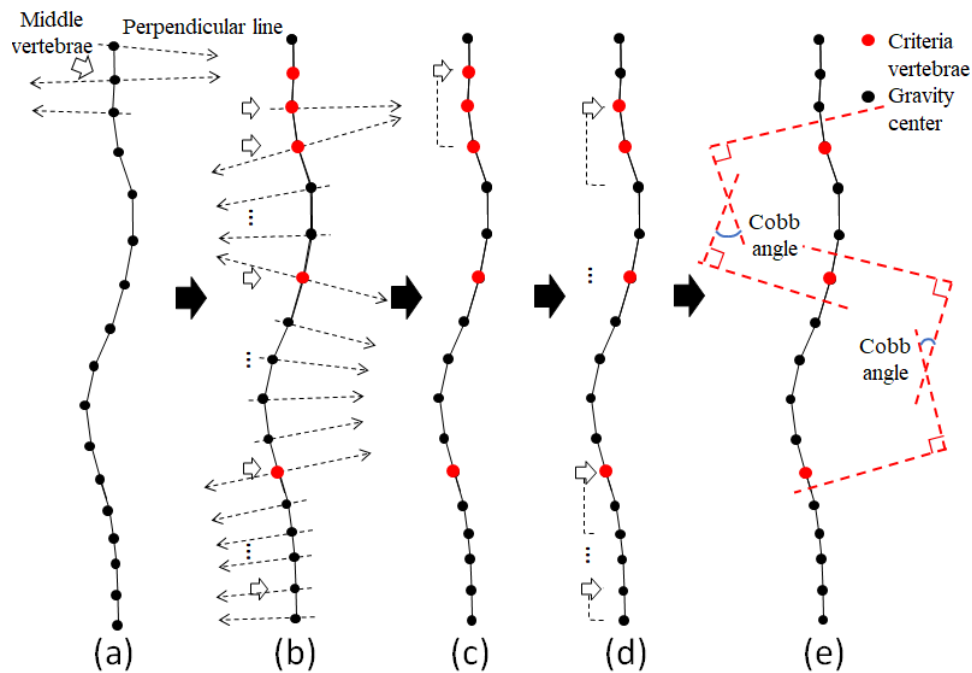


**Figure 4-2** Proposed method of measuring Cobb angle

2) Calculate the two contact points of three lines perpendicular to the curve at three sequential vertebrae: upper, middle, and bottom (Figure 4-2, (a)).

3) Define the middle vertebra as the criterion vertebra where the side of the point of contact changes (Figure 4-2, (b)).

4) Structurally, the concavity of the spinal curve is composed of more than four vertebrae including two criterion vertebrae at both ends of the curve. However, the curve using cubic

B-spline is slightly anfractuous because the spine is the estimated result (Figure 4-2, (c)). The criterion vertebra is redefined as a normal vertebra when other criterion vertebrae located on the lower level are located closer than the three vertebrae at the location of the criteria vertebrae. This step is implemented from T1 (the highest level) to L5 (the lowest level) in order of the vertebral level (Figure 4-2, (d)).

---

5) Calculate the angles between the two lines perpendicular to the curve at the midpoint between the top criterion vertebra and the vertebra above it, and at the mid-point between the bottom criterion vertebra and the vertebra below it (Figure 4-2, (e)).

In step 1), the cubic B-spline [Knott, 2012] was used to make the curve, which goes through every given point. Figure 4-3 shows the curve fitted by four methods, straight line, Bezier curve, mono curve and the cubic B-spline curve. The spinal curve has to be a soft curve showing enough curvature because we used the inflection point on the curve to calculate the Cobb angle.

Steps 1) - 3) are for finding the inflection points. We used the contact points of the perpendicular lines to find the inflection points fast only using 17 points. In step 4, the error is removed. Occasionally, the spinal curve has a zigzag shape, particularly when the spine has a small curve as shown in (b) and (c) of Figure 4-4. This step removes the criterion vertebrae located consecutively on the vertebral level. In step 5, we used the midpoint, which is equidistant from the upper and the lower side of vertebral block, instead of the criterion point located on the gravity center. Thus, the angle obtained using this measuring method was more similar than that found in the doctor's result.

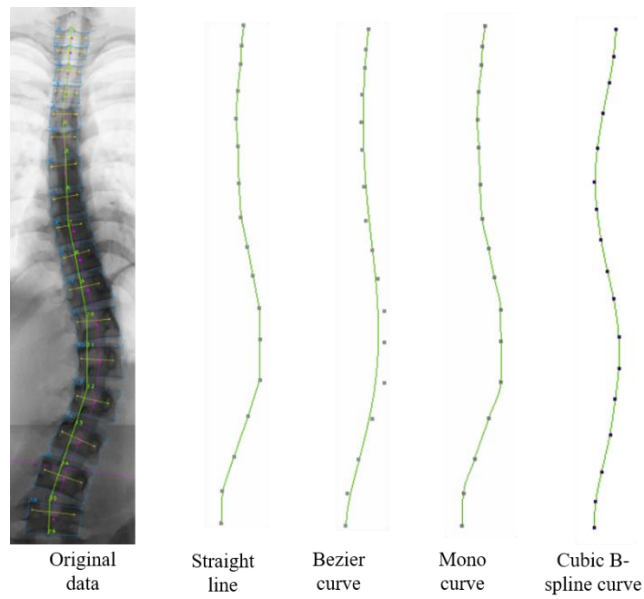


**Figure 4-3** Curve fittings

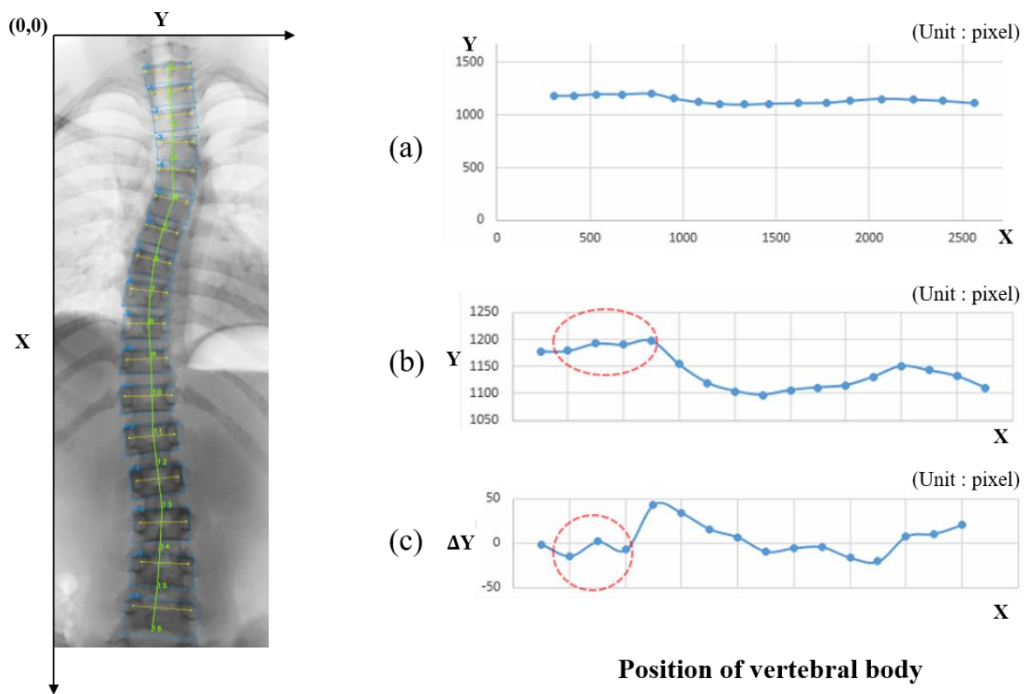


**Figure 4-4** Center position of the vertebral body

### 4.1.1 Validation of the proposed Cobb method

For validation of the method, we collected spinal features as we explained in Section 3, with Cobb angles measured by doctors. Based on the same data, we compared two Cobb angles obtained by doctors and the proposed Cobb method. The Cobb angle measured by a doctor, in many cases, was marked as  $0^\circ$  if the spine was normal. However, sometimes it was not  $0^\circ$  but lower than  $10^\circ$ . This angle was measured only for the large angles, and small Cobb angles tended to be ignored if the spine was abnormal because the spinal deformity is diagnosed by the largest angle. For this reason, only the biggest angle was used for the validation as shown in Figure 4-5.

The dataset that we used for validation included 1680 teenagers, 1410 females and 270 meals. The mean of weight was 45.9 kg (range: 21-79 kg), and height was 157 cm (range:

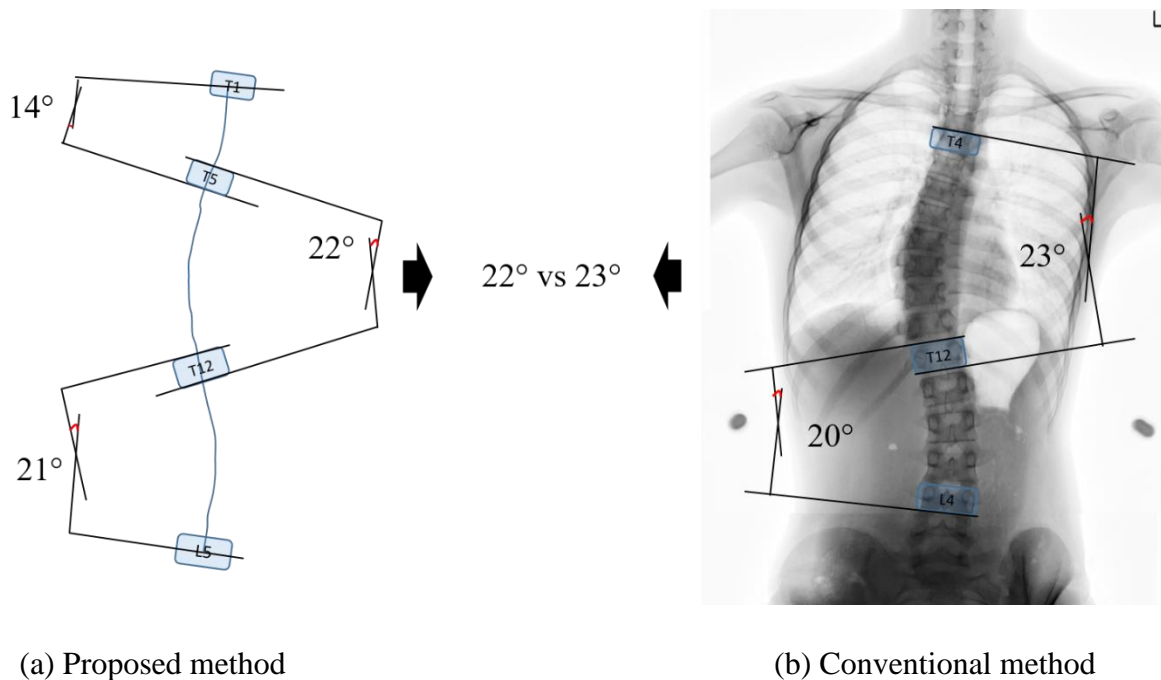


**Figure 4-5** Cobb angle comparison

128-180.4 cm). In the collected data, normal spines (Cobb angle  $< 10^\circ$ ) were 175, mild deformities ( $10^\circ \leq$  Cobb angle  $< 20^\circ$ ) were 890, and severe deformities ( $30^\circ \leq$  Cobb angle) were 622.

In comparison results as shown in Table 4-1, the MAE of a normal spine was  $3.13^\circ$ , the MAE of a spine with mild deformity was  $2.98^\circ$  and the MAE of a spine with severe deformity was  $2.78^\circ$ . The correlation infers that the MAE increases when the angle obtained by the doctor is smaller. Similarly, the spines with larger deformities had lower MAEs because of the clear criteria. This is owing to the observer variability of the Cobb angle measurement. It is harder to measure the Cobb angle on a straighter spine. The Accuracy of the angle is also influenced by the experience of the doctor, quality of the radiograph, and judgment of the observer. Observer error has been reported to vary from  $3^\circ$  to  $10^\circ$ .

The results of the automatic measurement of Cobb angle from the X-ray in other research [Sardjono et al., 2013] has reported a MAE of  $3.91^\circ$  with a standard deviation of  $3.60^\circ$  as shown in Table 4-1. In comparison with these results, the proposed method had a smaller error.

The Pearson correlation coefficient ( $r$ ) of entire vertebrae was high at 0.882 ( $p < 0.05$ ) and Figure 4-6 shows the graph. The Bland-Altman method was applied to access the agreement

**Table 4-1** Cobb angle error of the proposed method and comparison with another method

	MAE	SD
ALL	$2.9^\circ$	$2.54^\circ$
Normal	$3.13^\circ$	$2.76^\circ$
Mild deformity	$2.98^\circ$	$2.51^\circ$
Severe deformity	$2.78^\circ$	$2.47^\circ$
Sardjono method	$3.91^\circ$	$3.6^\circ$

between two Cobb angles. Through the Bland-Altman, the difference between two methods can be analyzed [Bland et al., 1986, Giavarina, 2015]. The average of the difference (called bias) was 1.57 and, the 95% limits of agreement were 8.4 and -5.3. The Bland-Altman plot is shown in Figure 4-6. When the average Cobb angle was changed, the difference (error) did not decrease or increase evidently. Thus, the plot means that the difference (error) had a steady distribution.

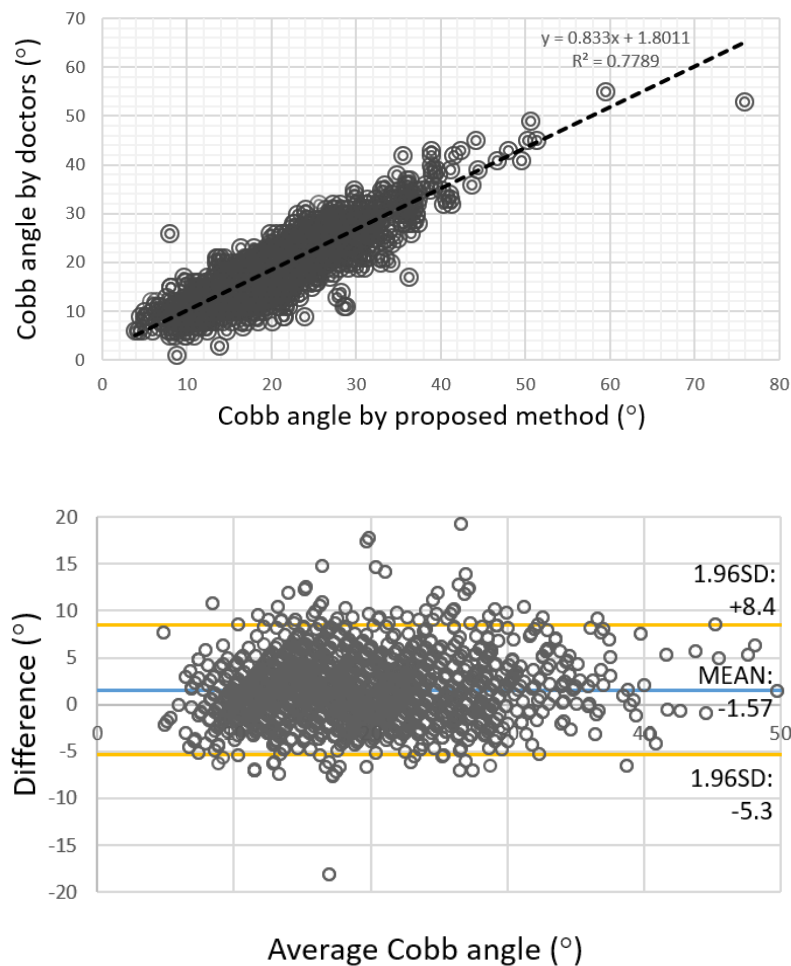
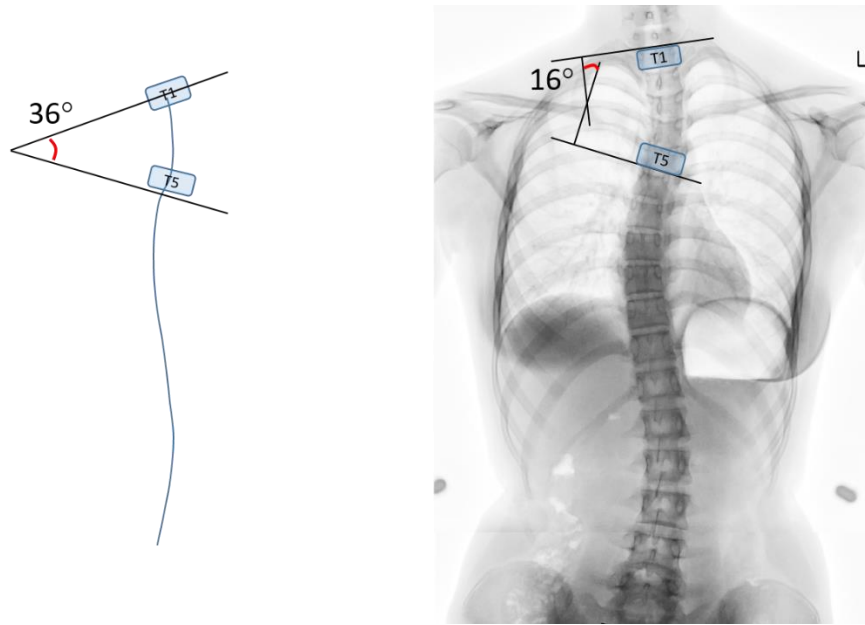
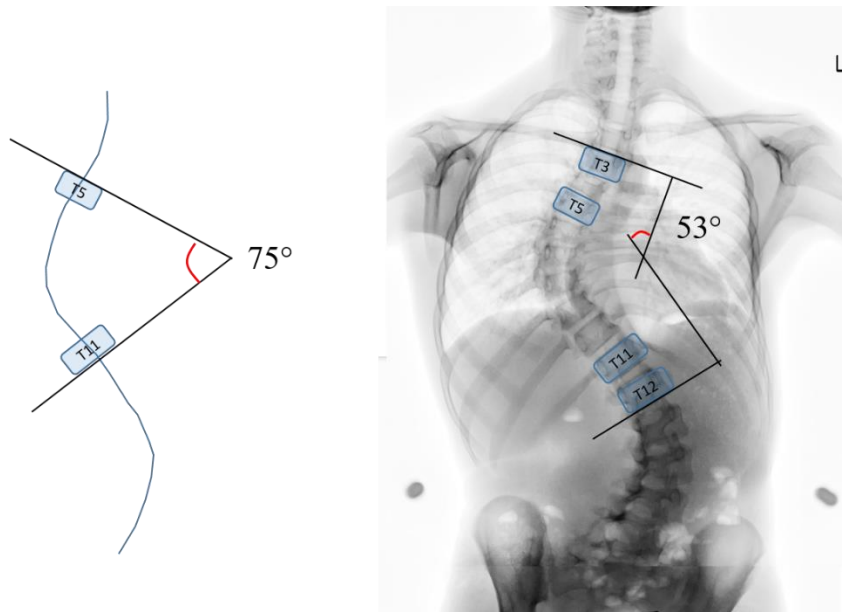


**Figure 4-6** Correlation (top) and Bland-Altman plot (bottom) between Cobb angles measured by doctors and by the proposed method



(a) Criteria position at the end of the spine



(b) Observer error

**Figure 4-7** The worst results in comparing two Cobb angles obtained by a doctor (right) and the proposed method (left)

Accordingly, our method was valid, having high correlation coefficient and small MAE in comparison with the ground truth. In addition, our MAE was smaller than the reported observer error.

#### 4.1.2 Limitation of the proposed Cobb method

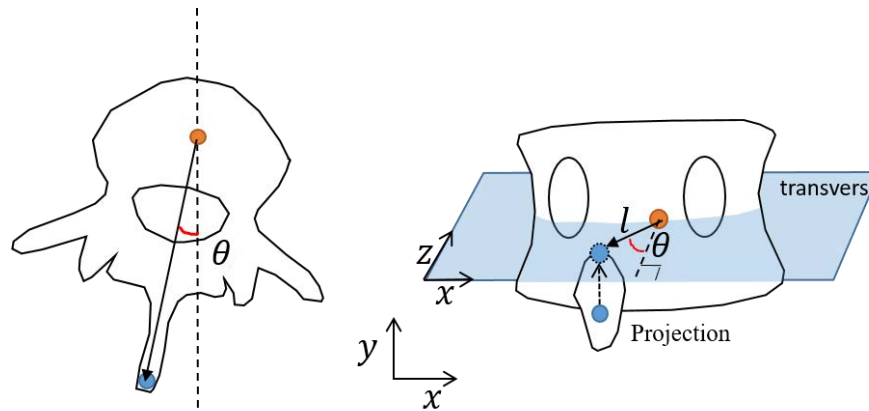
We compared two Cobb angles measured by doctors and the proposed method. To investigate the cause of a large error, we analyzed the worst results when comparing these two angles.

The first reason was that the criterion vertebra was at both ends of the spine such as T1 or L5. The proposed Cobb method used only centers of vertebral bodies but doctors measured Cobb angles based on the edges of the vertebrae. Therefore, there was the difference by the position of criteria as shown as (a) in Figure 4-7.

The second reason was by the observer error. Such as (b) in Figure 4-7, the criteria vertebrae of the proposed method were T5 and T11, whereas the criteria vertebrae of doctors were T3 and T12. When you see the spinal curve on the left side of Figure 4-7 (b), the inflection points are located closer to T5 and T11, not doctor's criteria T3 and T12. In case of (b), which had a large curve on the spine with the observer error, it was not used as data for the validation of the proposed method.

### 4.2 proposed method for measuring AVR

In this thesis, the angle of vertebral rotation (AVR,  $\theta$ ) is the angle formed by a vertical line and the line connecting the center of vertebral body and the tip of the spinous process, in a transverse plane as shown in Figure 4-8 (a). The vertical line is referenced from the coordinate of the Moire image. We only had 2D (x, y) data in a coronal plane and no (z) depth which is a necessary value for calculating AVR in the transverse plane. A general



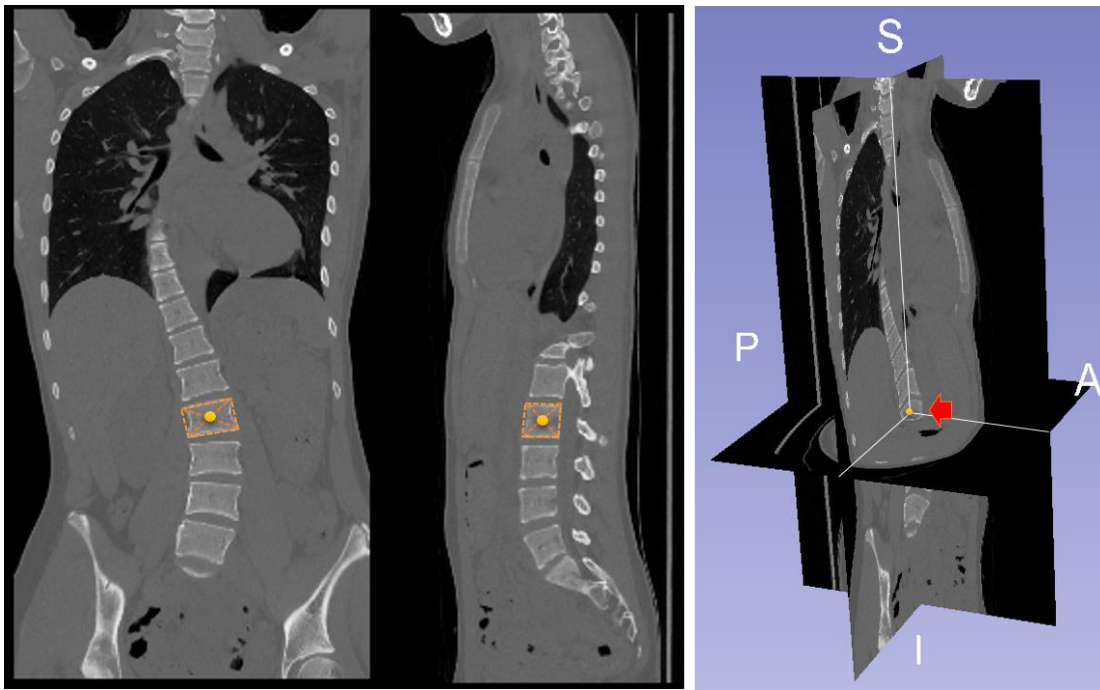
(a) Definition of AVR      (b) Method for measuring AVR from a 2D image

**Figure 4-8** 3D method (the ground truth) and 2D method for measuring AVR

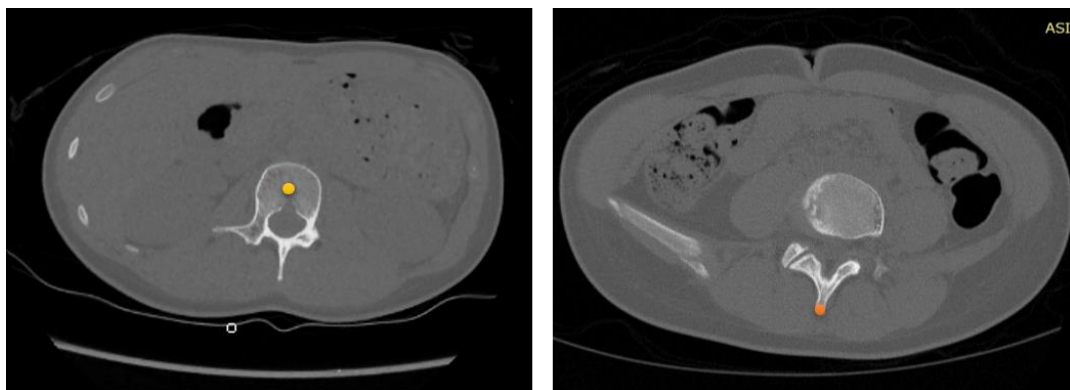
spinal dimension model is useful for referencing the distance between the center of the vertebral body and the tip of the spinous process. Thus, AVR is calculable based on the length ( $L$ ) obtained from the spinal model by a trigonometric function as shown in Figure 4-8 (b).

#### 4.2.1 Dataset for the spinal modeling

Since there exists no data pertaining to the spinal dimensions in growing teenagers [Zhou at al., 2000, Kunkel at al., 2010], we generated a general model of spinal dimensions based on CT data. The data were obtained from 20 teenagers (19 females, and 1 male) with severe AIS. The mean age of the teenagers was 15 years (range: 11-19 years), weight was 44.2 kg (range: 33-56 kg), and height was 158 cm (range: 151.2-170.7 cm). The collected data from CT consisted of the center of the vertebral body and the tip of the spinous process. The center of the vertebral body was the center point of vertebral block in both planes, coronal and sagittal like (a) and (b) in Figure 4-9. (c) in Figure 4-9 shows the collected point, one center of the vertebral body. The tip of the spinous process was collected in the transverse plane.



(a) Center of vertebral body in the coronal plane (b) Center of vertebral body in the sagittal plane (c) Center of vertebral body in the three planes



(d) Center of vertebral body in the transverse plane

(e) Tip of spinous process in the transverse plane

**Figure 4-9** One center point of vertebral body and one tip of spinous process collected from CT image slice

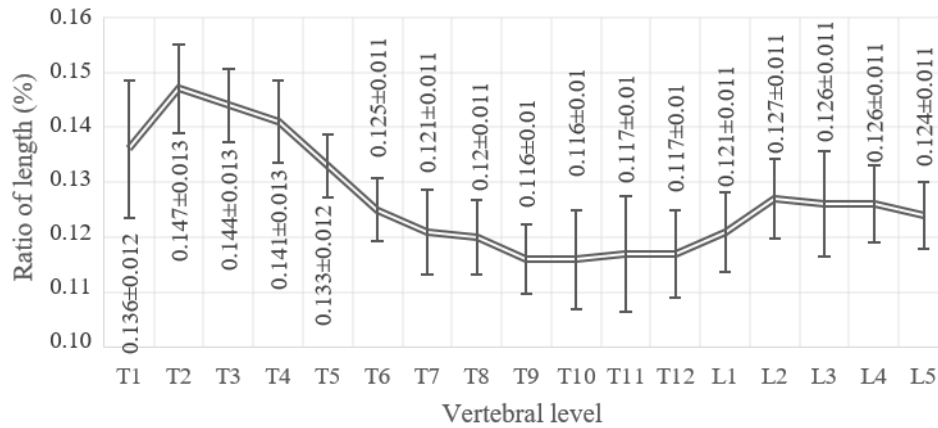


**Figure 4-10** Spinal dimensions of each vertebra

To collect the points, we used 3D slicer [Fedorov et al., 2012]

These data were analyzed after converting into a ratio divided by the spinal length (see Figure 4-10). L indicates a length when the spinal length is 1; therefore, the L was applied after conversion to an actual length multiplied by the spinal length. VRA was calculated by  $\sin^{-1}(\Delta x/L)$ , and the programmed result was a negative value when the vertebra is twisted clockwise, and a positive value when twisted counter-clockwise.

#### 4.2.2 Validation of the proposed AVR method

Based on the same data, we compared AVR results obtained by two methods, one is a 3D AVR method (the ground truth) for measuring AVR using  $(x, y, z)$  coordinates like (a) in Figure 4-8, and the proposed method measuring AVR using  $(x, y)$  coordinates and the spinal dimension model like (b) in Figure 4-8. Both methods used same feature points, the tip of the spinous process and the center of the vertebral body. The used dataset was CT data of 6 females with

severe AIS, aged 10-15, and mean height of dataset was 156 cm. The MAE for the entire vertebrae (n=102, 6x17) was  $0.49^\circ \pm 0.81^\circ$  as shown in Table 4-2.

MAE of each AVR range, categorized by the angle obtained by 3D AVR method, were  $0.11^\circ \pm 0.14^\circ$ ,  $0.38^\circ \pm 0.46^\circ$ ,  $0.51^\circ \pm 0.63^\circ$  and  $1.76^\circ \pm 1.7^\circ$  for absolute AVR of  $0.0^\circ \sim 5.0^\circ$ ,  $5.0^\circ \sim 10.0^\circ$ ,  $10.0^\circ \sim 15.0^\circ$  and  $>15.0^\circ$  respectively, as shown in Table 4-2.

MAE and average absolute AVR of each vertebral level are shown in Figure 4-11. Both results, Table 4-2 and Figure 4-11, show that when absolute AVR was large, the MAE was large.

Ultrasound method [Wang et al., 2016] compared two methods, their Ultrasound method and a MRI method as the ground truth. To measure VR, the ultrasound method used centers of laminae and a reference line, and the MRI method used the posterior junction of the two laminae and the reference line. The MAE between the two methods reported  $0.3^\circ \pm 0.3^\circ$ ,  $0.5^\circ \pm 0.3^\circ$  and  $1.0^\circ \pm 1.1^\circ$  for AVR of  $0.0^\circ \sim 5.0^\circ$ ,  $5.0^\circ \sim 10.0^\circ$  and  $10.0^\circ \sim 15.0^\circ$  respectively, as shown in Table 4-2. We compared two MAEs, obtained from the proposed method versus 3D AVR (the ground truth) and the Ultrasound method versus the MRI method, to verify the magnitude of MAE is small or large, not for the accuracy of the methods. The MAE between the proposed method versus the 3D AVR was smaller than the MAE between the Ultrasound method versus the MRI method.

The Pearson correlation coefficient (r) of entire vertebrae was very high at 0.996 ( $p < 0.05$ ) and Figure 4-12 shows the graph. In addition, the Bland-Altman method was applied to assess the agreement between two methods, the proposed method and the 3D AVR method. The average of the difference (bias) was -0.2 and, the 95% limits of agreement were 1.72 and -1.98. The Bland-Altman plot is shown in Figure 4-12, and the plot means that the error between the ground truth and the measured AVR, is large when the average absolute AVR is large.

Accordingly, our method was valid, having a high correlation coefficient with the ground truth. In addition, MAE was larger when AVR was large.

**Table 4-2** MAE between the proposed method and 3D AVR method (the ground truth), and MAE in another reference [Wang at al., 2016] between Ultrasound method and MRI method

Range	MAE	MAE of Wang's method
All	$0.49^\circ \pm 0.81^\circ$	-
$ \text{AVR}  < 5^\circ$	$0.11^\circ \pm 0.14^\circ$	$0.3^\circ \pm 0.3^\circ$
$5 \leq  \text{AVR}  < 10^\circ$	$0.38^\circ \pm 0.46^\circ$	$0.5^\circ \pm 0.3^\circ$
$10 \leq  \text{AVR}  < 15^\circ$	$0.51^\circ \pm 0.63$	$1.0^\circ \pm 1.1^\circ$
$15 \leq  \text{AVR} $	$1.76^\circ \pm 1.7$	-

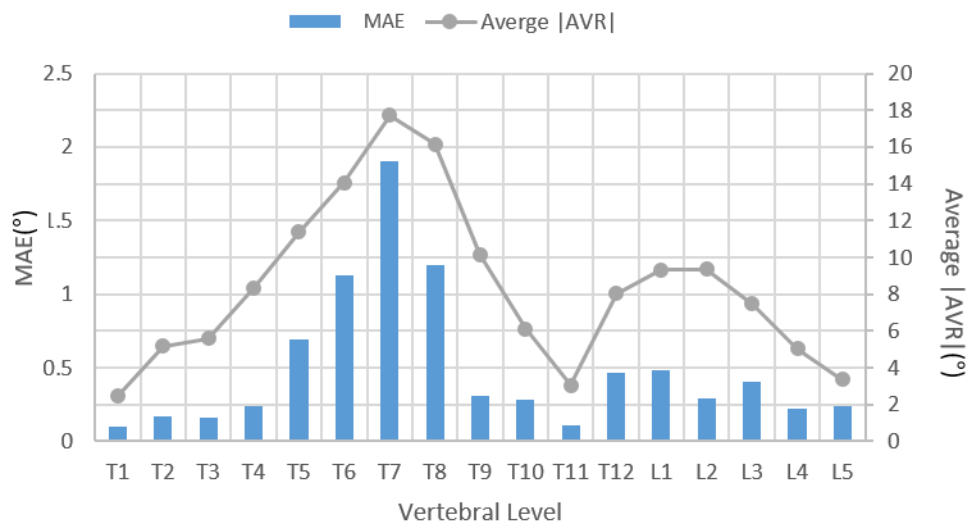


**Figure 4-11** MAE and Average absolute AVR of each vertebra

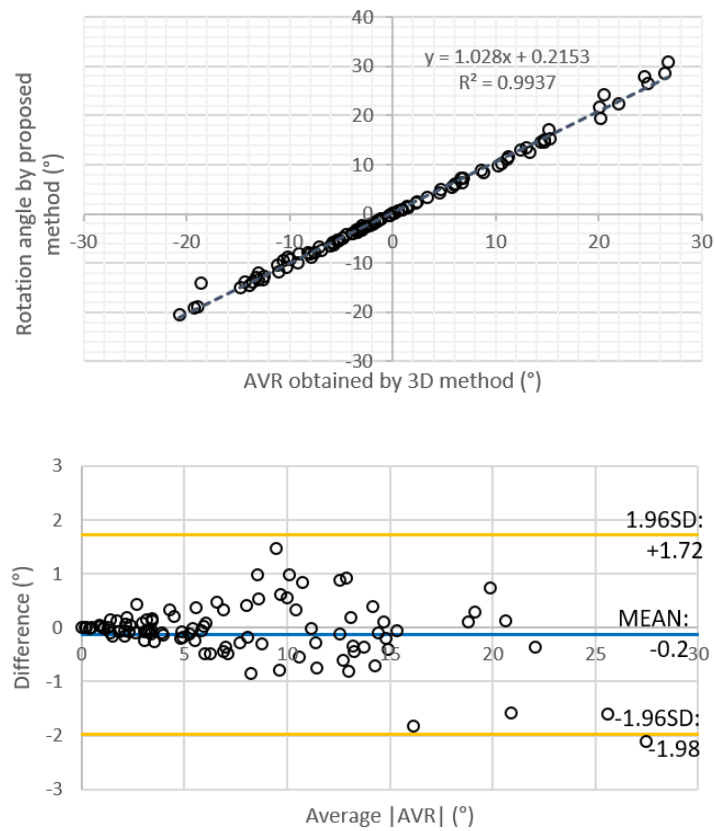


**Figure 4-12** Correlation (top) and Bland-Altman plot (bottom) between the proposed method and 3D AVR method

## Chapter 5

# Spine Estimation from Moire image

We estimate the spine shape by CNN, and evaluate it by two proposed measuring method for the Cobb angle and AVR, which were introduced in Section 4. A network of CNN that we used is described in Section 5.1. In Section 5.2, we describe datasets used for the training and test, and in Section 5.3, we describe the experiment result evaluated by the proposed measuring methods.

### 5.1 Networks of CNN

To estimate the spine shape, we used a relatively shallower network, AlexNet [Toshev et al., 2014], than other networks such as ResNet. Year by year, a network model is getting deeper and deeper with better performance [Krizhevsky et al., 2012, He et al., 2016, He et al., 2016, Oct.]. However, in all cases, the use of the deeper network does not improve performance.

The deeper networks are more difficult to train due to a complexity increased by increased parameter by adding layers. Thus, a small dataset is not enough information to optimize the parameters [Goodfellow et al., 2016]. We used dataset of 1965 which is respectively much smaller than another research using over 1,280,000 labeled images [Krizhevsky et al., 2012].

The architecture of the CNN is based on reference [Toshev et al., 2014] as shown in Figure 5-1. AlexNet is a network architecture comprising five convolutional layers (C) and two fully connected layers (FC). C describes (width x height x depth) and FC describes (Depth) in Figure 5-1. The width and height mean the filter size, and the depth means the number of filters. F means a filter showing as yellow rectangles in Figure 5-1 for the convolution, and is describe as (width x height, stride, padding). Max pooling is applied (3x3, s:2) to downscale of the feature map. The Max pooling operates in order that output has the max value in the respective filter. Here, the stride is a step of convolution over the input and the padding is a volume increasing the input size by adding 0. As an activation function for neural networks, we used a rectified linear unit (ReLU), which is effective for convergence performance and learning speed.

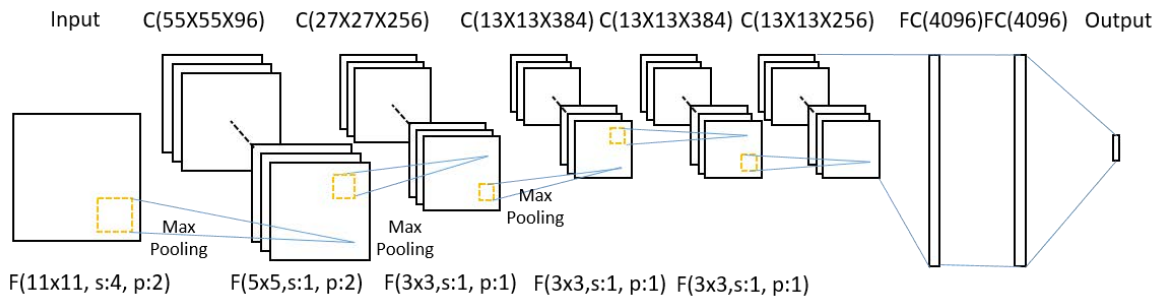


**Figure 5-1** Architecture of CNN used in this thesis

### 5.1.1 Network structure to estimate the spine

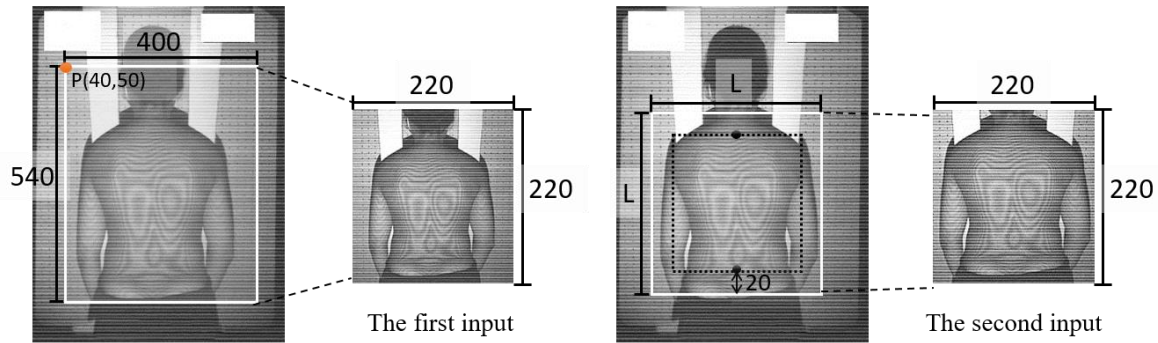


**Figure 5-2** Input images for the first and second CNNs

We used two CNNs, one is for extracting a back area from the Moire image, and another one is for estimating spinal positions from the back area as shown in Figure 1-6.

Before the Moire image was input into the CNN, the image was processed; the histogram was equalized to adjust the contrast, and a Fourier transformation was completed to remove noise. The Fourier transformation removed low frequencies by masking using a  $100 \times 100$  rectangular window.

Figure 5-2 shows two inputs for the net. The input of the first CNN was an image that was cropped from the original image ( $480 \times 640$ ) to size  $400 \times 540$  at a fixed position with the top-left corner  $p(40, 50)$ , and then resized to  $220 \times 220$ . We cropped the image to size  $400 \times 540$  to cut needless parts like the background as well as to response various heights of teenagers. The back of human on the Moire image was about  $240 \times 300$  size that is less half size of the original image. In addition, teenagers differed in heights, but the viewpoints of Moire camera were always in the same position during the screening. Therefore, the input size was determined on the size  $(400 \times 540)$  which can be response for all back areas in the dataset, in spite of the ratio of the image is changed. The output of the first CNN was two tips of spinous

processes on the first and last vertebrae, T1 and L5. These two tips are easy to detect by appearing on the back surface.

The input of the second CNN was the Morie image which cut based on the two the tips detected by the first CNN. A center of the two tips was centered on the cropped image and cut to the size, spine length + padding (20 pixels), and then resized to 220×220. The output of the second CNN was 34 spinal positions, the tip of the spinous process and the center of the gravity center of 17 vertebrae blocks.

## 5.2 Dataset

For the dataset, we collected 1965 pairs of Moire and X-ray images. These data were obtained from teenagers, aged 11–16 years, with Cobb angles ranging from 0° to 55°. The collected spinal information comprised two features: a center of the vertebral body and a tip of the spinous process on one vertebra, as well as 12 thoracic (T1-T12) and 5 lumbar (L1-L5) vertebrae.

We divided the dataset into 200 data series for the test dataset and 1765 for the training dataset. The test dataset comprised 66 normal data series (Cobb angle < 10°), 70 data series with mild deformities (10° ≤ Cobb angle < 20°), and 64 data series with severe deformities (20° ≤ Cobb angle). To avoid overfitting problem during the training, the training dataset augmented to 36652 by rotation (5° clockwise and anticlockwise) and mirroring.

## 5.3 Result evaluation

Figures 5-3, 5-4, 5-5 show the ground truths and the estimated results. From the left side, there are results of the first CNN, results of the second CNN, and the ground truth. Each Figure shows according to the three deformity levels, Figure 5-3 for the normal spine, Figure

5-4 for the spine with mild deformity, and Figure 5-5 for the spine with severe deformity. The result of the first CNN is the back area shown by yellow rectangle based on two end tips of the spinous process. The result of the second CNN is 34 points. The numbers under the second CNN result are Cobb angles obtained by the proposed method, and the numbers under the ground truth are obtained by doctors based on the X-ray. The graph on the Moire images shown by the orange line means the AVR of each vertebra. Black lines on the center of Moire image are lines connecting the 17 centers of the vertebra bodies. White lines on the black line are lines connecting two points, the center of the vertebra body and the tip of the spinous process.

The spinal curves connecting the centers of the vertebra body on the results had similar curve shapes on the ground truth. Furthermore, the curves on the results shown more natural curves than the spinal curves on the ground truths. The curve shapes on the ground truth and estimation result had similar curvature.

As shown in Table 5-1, MAE of the first CNN was  $4.14 \pm 2.5$  pixel. In comparing MAEs of each deformity, normal spine (Cobb angle  $< 10^\circ$ ) was  $4.05 \pm 2.24$ , mild deformity ( $10^\circ \leq$  Cobb angle  $< 20^\circ$ ) was  $4.01 \pm 2.56$ , severe deformity less than  $30^\circ$  ( $20^\circ \leq$  Cobb angle) was  $4.46 \pm 2.67$ , and severe deformity over  $30^\circ$  ( $30^\circ \leq$  Cobb angle) was  $4.04 \pm 2.56$ .

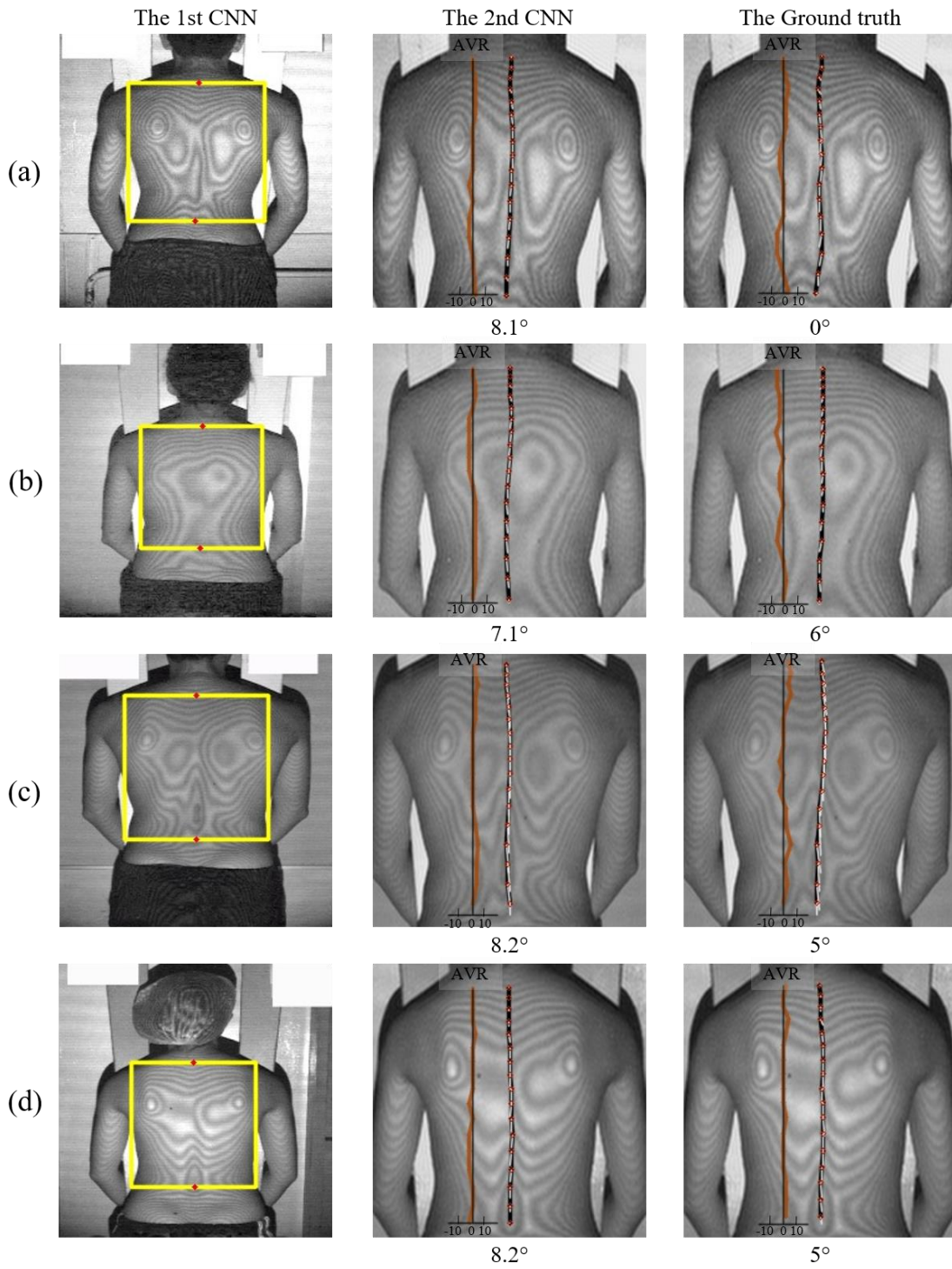
The MAE of the second CNN was  $4.06 \pm 2.52$  pixels ( $4.08 \pm 2.56$  mm). In comparing results of two different features, the tip of spinous process had a slightly smaller MAE ( $3.99 \pm 2.58$  pixel) than the center of the vertebral body ( $4.12 \pm 2.47$  pixel). Figure 5-3 shows the MAE of each feature according to each vertebra level. Considering the MAEs of each vertebra, it is not seen that either of two features has a better estimated result.

In comparing results of four deformity levels, MAE of each was  $3.79 \pm 2.33$  for normal,  $3.85 \pm 2.28$  for mild deformity,  $4.42 \pm 2.77$  for severe deformity smaller than  $30^\circ$ , and  $4.98 \pm 3.12$  for severe deformity larger than  $30^\circ$ . The MAE was large in case of the severe deformity, whereas, The MAE for the normal and the mild deformity were similar. It considered that estimation was difficult because Moire pattern of severe deformity is various

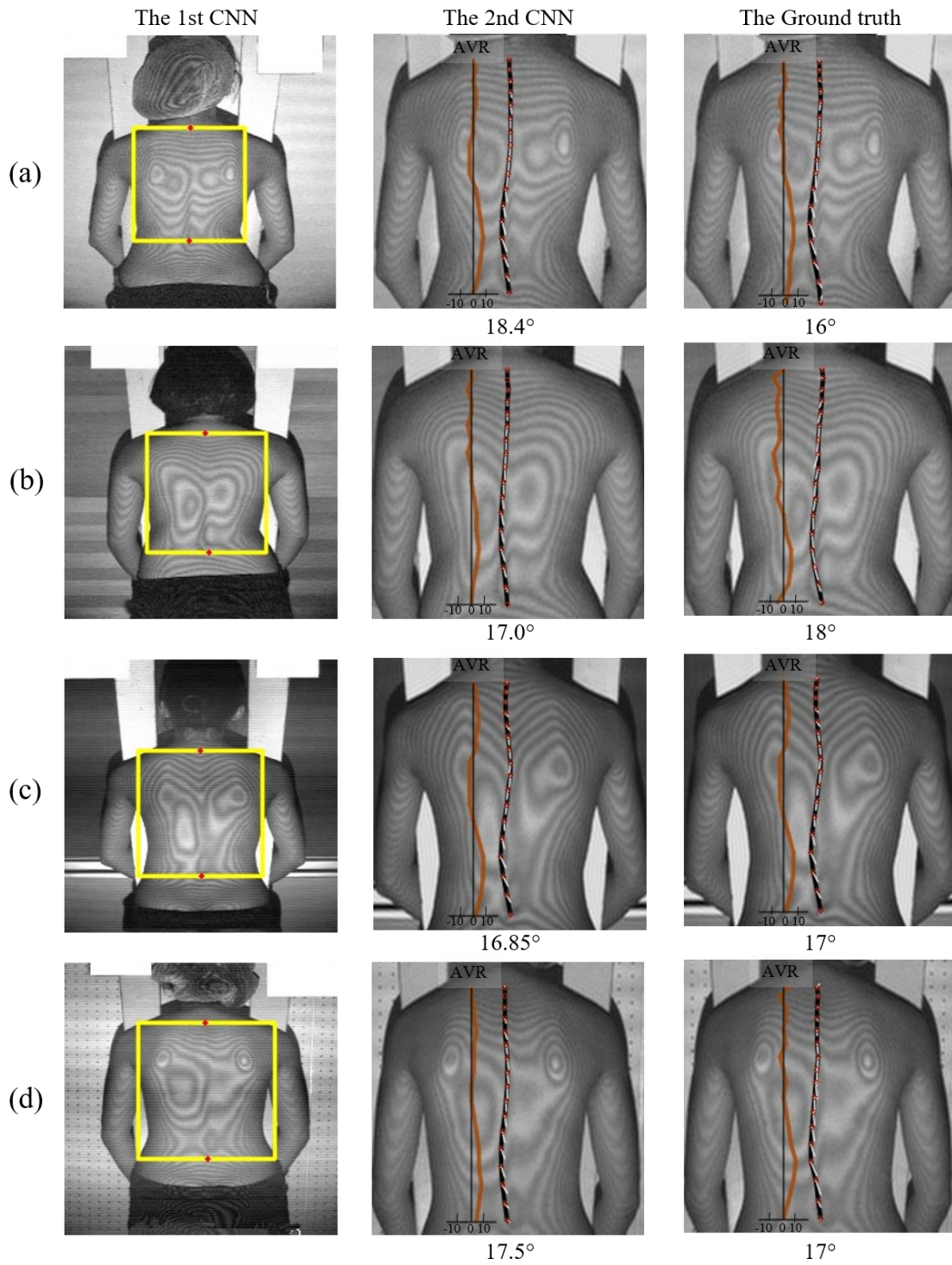
and also, the number contained in the dataset was same with other levels although the range of Cobb angle was large from 20° to over 50°.

Figure 5-6 shows MAE of each 17 vertebrae relative to each feature. Relatively, the estimation having a low MAE was the first and last vertebrae, T1 and L5, and the estimation having a large MAE was vertebrae in the center such as T8 to T12. It is because T1 and L5 are at the center of the neck and pelvis, and T8 to T12 are in an area where the variation of spine shape is large.

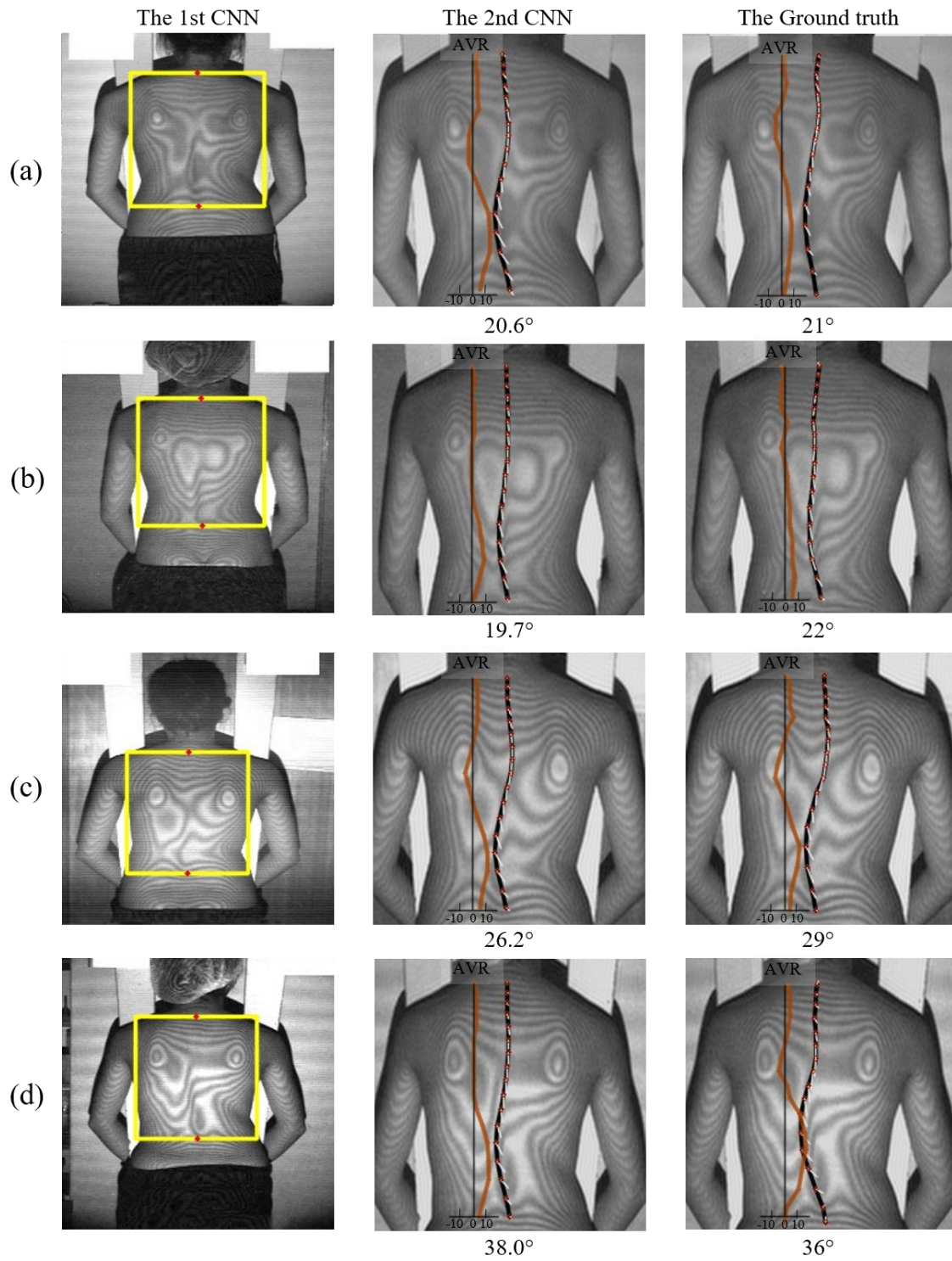
To evaluate the estimated result concretely, Cobb angle and AVR were compared with the ground truth in Section 5.3.1 and 5.3.2.



**Figure 5-3** Estimated result of the normal spine



**Figure 5-4** Estimated result of the spine with mild deformity

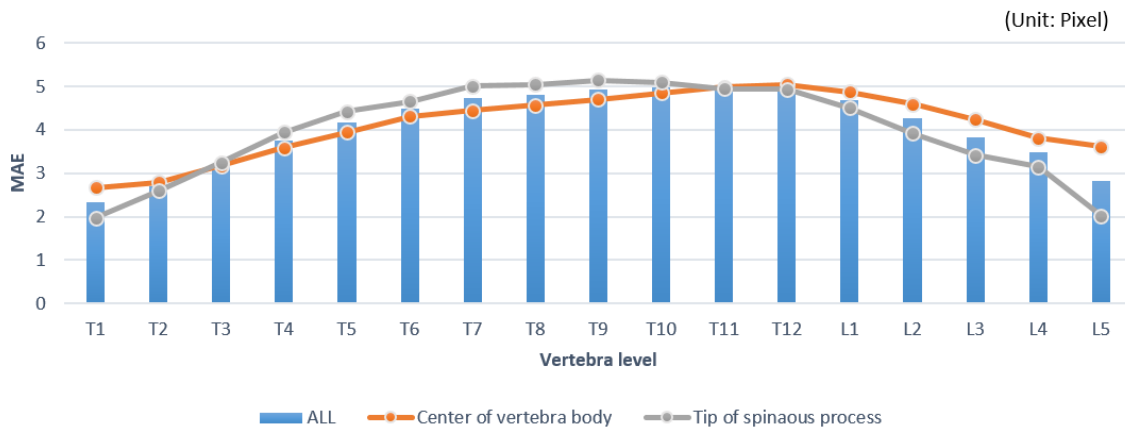


**Figure 5-5** Estimated result of the spine with severe deformity

**Table 5-1** MAE of the estimated position

(Unit: pixel)

	MAE of the first CNN	MAE of the second CNN
All	$4.14 \pm 2.5$	$4.06 \pm 2.52$ ( $4.08 \pm 2.56$ mm)
Center of vertebral body	-	$4.12 \pm 2.47$ ( $4.15 \pm 2.51$ mm)
Tip of spinous process	-	$3.99 \pm 2.58$ ( $4.01 \pm 2.56$ mm)
Normal (Cobb angle $< 10^\circ$ )	$4.05 \pm 2.24$	$3.79 \pm 2.33$ ( $3.74 \pm 2.28$ mm)
Mild deformity ( $10^\circ \leq$ Cobb angle $< 20^\circ$ )	$4.01 \pm 2.58$	$3.85 \pm 2.28$ ( $3.87 \pm 2.30$ mm)
Severe deformity ( $20^\circ \leq$ Cobb angle $< 30^\circ$ )	$4.46 \pm 2.67$	$4.42 \pm 2.77$ ( $4.50 \pm 2.91$ mm)
Severe deformity ( $30^\circ \leq$ Cobb angle)	$4.04 \pm 2.56$	$4.98 \pm 3.12$ ( $5.04 \pm 3.21$ mm)

**Figure 5-6** MAE of each features according to each vertebra

### 5.3.1 Evaluation using the proposed method measuring Cobb angle

Cobb angles were measured based on the 17 centers of the vertebral bodies. After evaluation by the proposed method, the maximum Cobb angle on the one spine compared with the Cobb angle measured on X-ray image by doctors. It is because doctors diagnose as AIS using the largest Cobb angle.

The MAE of Cobb angle was  $3.8^\circ \pm 3.03^\circ$ . In this result as shown in Table 5-2, the MAE for each category was  $4.73^\circ \pm 3.26^\circ$  for normal spines,  $4.26^\circ \pm 3.53^\circ$  for spines with mild deformity,  $2.87^\circ \pm 2.02^\circ$  for spines with severe deformity smaller than  $30^\circ$ , and  $3.05^\circ \pm 1.52^\circ$  for spines with severe deformity larger than  $30^\circ$ . While the MAE of position for hard deformity had a large MAE, the MAE of Cobb tended to have a small error for hard deformity. It is considered that measuring criteria are clear when measuring the Cobb angle. The Cobb angle is the angle between two criteria. It is difficult to define the clear criteria on the spinal curve having almost straight line. On the other hands, it is easy to define criteria on the spinal

**Table 5-2** MAE of Cobb angle of estimated position

	MAE	SD
All	$3.80^\circ$	$3.03^\circ$
Normal ( $0^\circ < \text{Cobb angle} < 10^\circ$ )	$4.73^\circ$	$3.26^\circ$
Mild deformity ( $10^\circ \leq \text{Cobb angle} < 20^\circ$ )	$4.26^\circ$	$3.53^\circ$
Severe deformity ( $20^\circ \leq \text{Cobb angle} < 30^\circ$ )	$2.87^\circ$	$2.02^\circ$
Severe deformity ( $30^\circ \leq \text{Cobb angle}$ )	$3.05^\circ$	$1.52^\circ$

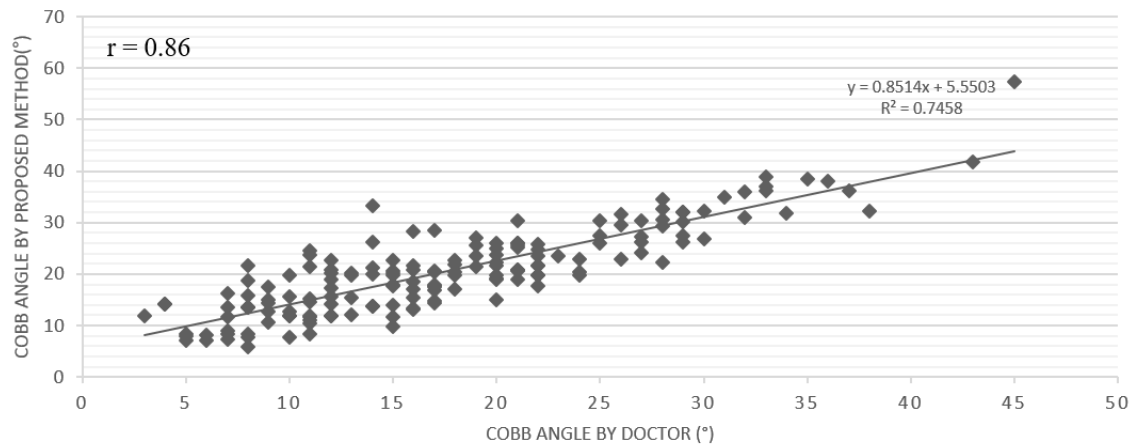


**Figure 5-7** Correlation between two Cobb angles measured by Doctor and the proposed method

curve having a hard curve. Thus, MAE became large by imprecise criteria in case of the normal spine. In results of the severe spine, the larger than  $30^\circ$  had large MAE than the smaller than  $30^\circ$  because the large deformity had a large MAE as shown in Table 5-1.

Figure 5- 7 shows the correlation between the maximum Cobb angles measured by doctors and the proposed method. The correlation coefficient ( $r$ ) was high at 0.86.

### 5.3.2 Evaluation using the proposed method measuring AVR

AVR was measured based on the 17 centers of the vertebral bodies and 17 tips of the spinous processes, and all 17 AVRs were on the one spine compared with the AVRs measured on the X-ray image.

As shown in Table 5-3, MAE of AVR was  $2.95^\circ \pm 2.7^\circ$ . Each MAE for absolute AVR of  $0 \sim 5^\circ$ ,  $5^\circ \sim 10^\circ$ ,  $10^\circ \sim 15^\circ$ , and larger than  $15^\circ$ , were  $1.93^\circ \pm 1.8^\circ$ ,  $2.57^\circ \pm 2.18^\circ$ ,  $3.24^\circ \pm$

2.63° and  $5.06° \pm 4.66°$  respectively. The MAE of absolute AVR tended to have large MAE if absolute AVR was large.

Figure 5-8 shows MAE of AVR according to the vertebral level. L2 and L3 had a large average absolute AVR, while MAEs of AVR had similar values without large fluctuations despite the change of vertebra level.

Figure 5-9 shows the correlation between the Cobb angle and AVR. Here, both values used the maximum values in one spine. For pathological diagnosis, important results belonged to (a) and (b) are shown by yellow and blue rectangles. These are the spine with mild deformity, but not All of them are AIS. The Cobb angle over 10° is the standard of classification of AIS but actually the Cobb angle over 10° without rotation is not AIS as we explained in Section 1.2. The results of these are shown in Figures 5-10 and 5-11.

Figure 5-10 corresponds to (a) in Figure 5-9. The spine results in Figure 5-10 are the spine with mild deformity having a large AVR. In this case, a patient is required to get the treatment as following as general steps. Contrastively, the spine result in Figure 5-11 corresponding (b) in Figure 5-9 are the spine with mild deformity having a small AVR. In this case, a patient is required the monitoring because this case is considered as non-structural scoliosis, not AIS.

In this thesis, we could not compare the classified results of (a) and (b) whether AIS or not due to no ground truth by an unestablished standard for diagnosing. However, by supping the results belonging to (a) and (b), we presented the possibility for a subdivided diagnosis of scoliosis, structural or nonstructural scoliosis.

**Table 5-3** MAE of absolute AVR between the estimation petitions and the ground truth

	MAE	SD
All	2.95°	2.7°
$ AVR  < 5°$	1.93°	1.8°

$5^\circ \leq  AVR  < 10^\circ$	2.57°	2.18°
$10^\circ \leq  AVR  < 15^\circ$	3.24°	2.63°
$15^\circ \leq  AVR $	5.06°	4.66°



**Figure 5-8** MAE and average absolute AVR according to the vertebra level. Here, the absolute AVR is an average angle of ground truth and the estimated result

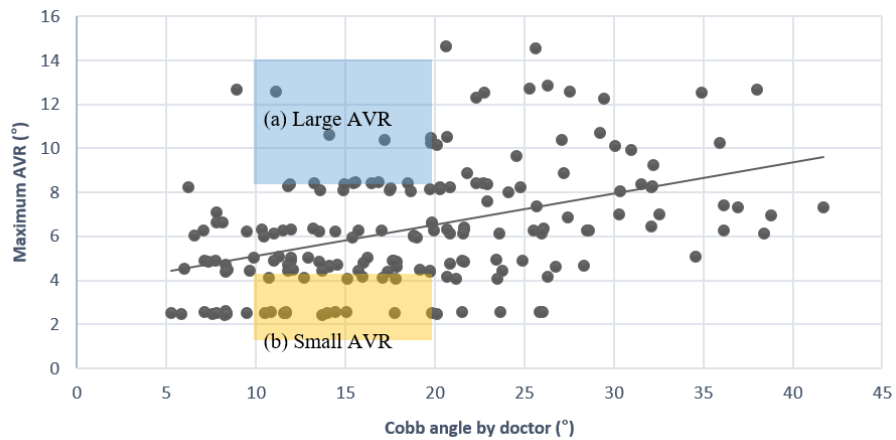
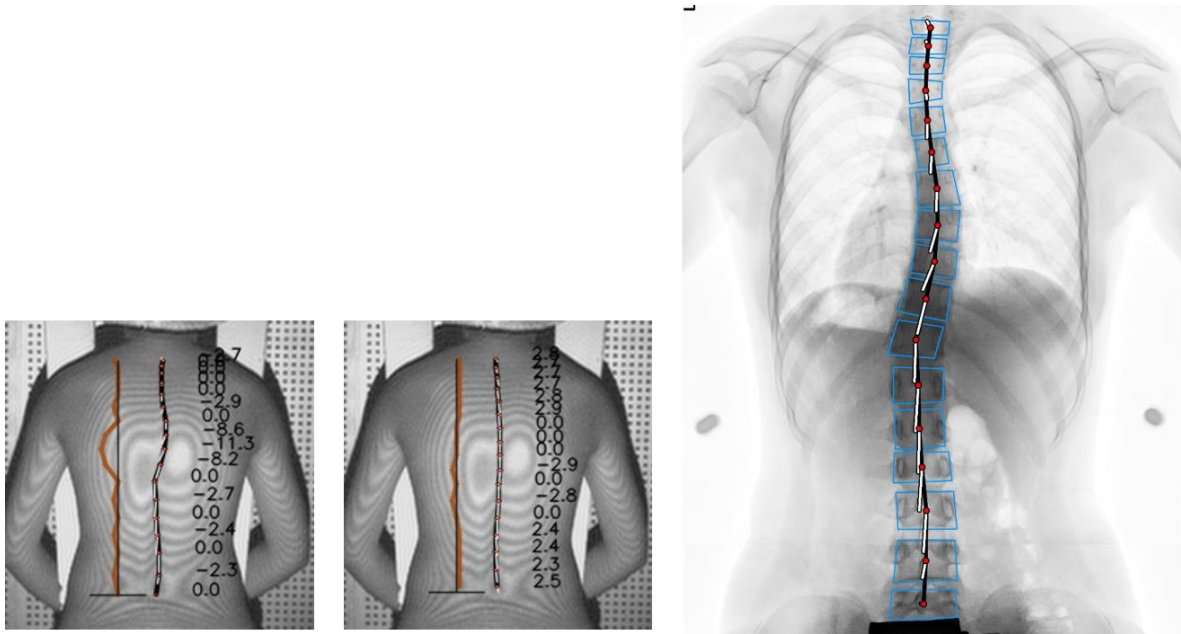


**Figure 5-9** Correlation between Cobb angle and AVR

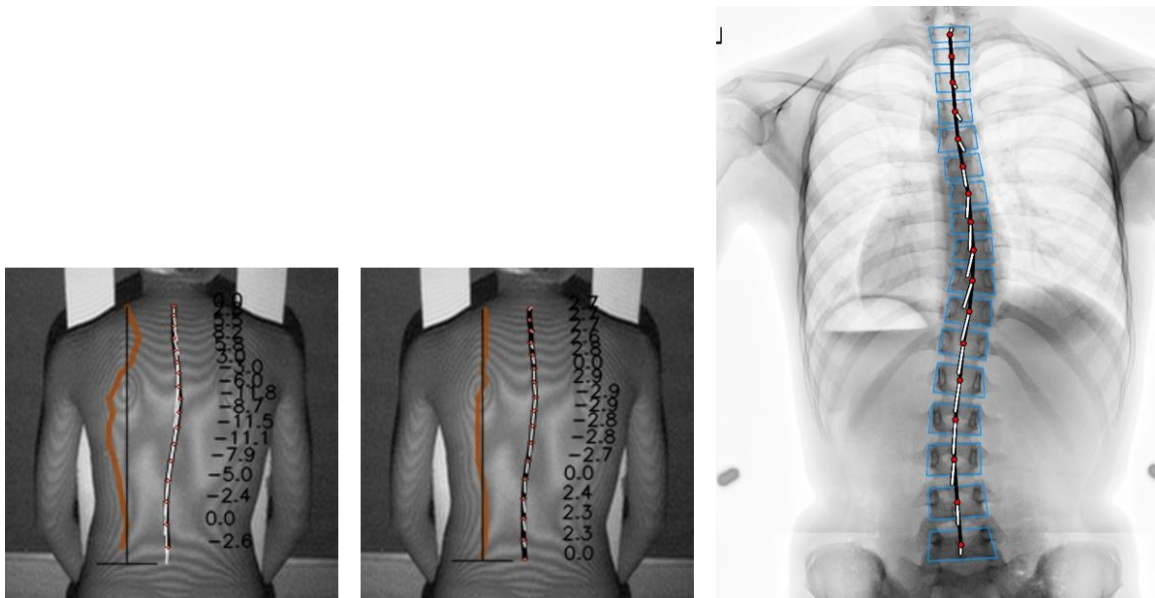




(a) Ground truth

(b) Estimated result

(c) X-ray image



(a) Ground truth

(b) Estimated result

(c) X-ray image

**Figure 5-11** Patients having small AVR

## 5.4 Conclusions of experiments

We extracted the back area and the spinal shape using two CNNs. In addition, we evaluated the estimated results by measuring Cobb angle and AVR.

In another study for the screening which reconstructed the 3D body for spine estimation and was also a previous paper for the current developed product [Hackenberg et al., 2002], The root mean square error (RMSE) was 4.4° or 5.8 mm. They evaluated the result of their system with real data, that condition was same as the proposed method, therefore we chose to compare. In comparison with this, our estimation error was small as shown in Table 5-4.

In the test dataset, some patients had specific Moire patterns by the body type as shown in Figure 5-12. Their body were fat and the area around the center of back surface was protruded. This specific pattern tended to estimate with low accuracy by CNN. The curve of the spine had an almost straight line like results of the 2nd CNN in Figure 5-12. Therefore, it means that additional research according to the body type is required for more accurate results.

**Table 5-4** Result comparison with another method

	RMSE
Our method	4.12°, 4.08mm
Hackenberg [Hackenberg at al., 2002]	4.4°, 5.7mm

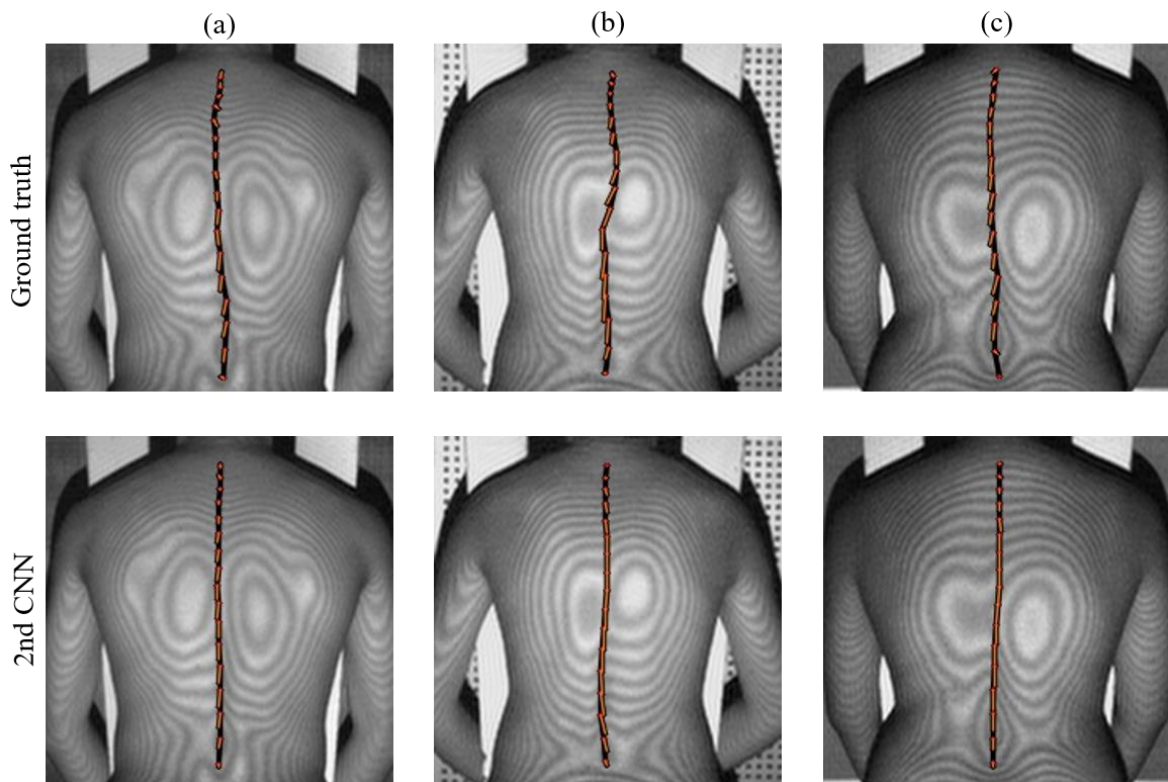


**Figure 5-12** Results by the specific Moiré pattern of fat patients

## Chapter 6

### Conclusion

We proposed an estimator measuring Cobb angle and the vertebral rotation of the spine from the Moire image.

The Moire and X-ray images of the same patient were collected to create a dataset. On a vertebra, a center of vertebral body with a tip of spinous process were detected as spine information and one spine consisted of 17 vertebrae. The dataset was generated by merging the Moire image and X-ray image, and perspective projection was applied to reduce the error caused by merging two images taken from different camera viewpoints.

Two CNNs were used to estimate the spine shape. The first one was used to estimate the back area from the Moire image. Then, the second one estimated spine positions from the back image. The estimated spine was evaluated by measuring Cobb angle and AVR.

In addition, the measuring method for calculating the Cobb angle and the AVR were

---

proposed for the spinal screening. As a result of the estimator, a spinal shape and indicators, Cobb angles and the AVR, were obtained. The obtained indicators were crucial values to diagnose AIS, which cannot obtain from the conventional screening methods. It is the different point from the conventional Moire methods that require an additional diagnosis by a radiographic method.

In comparison with the Cobb angle measured by doctors on the same X-ray, the Cobb angle obtained by the proposed measuring method had a smaller difference in angle than the error caused by observers. However, it tended to obtain a larger angle when the Cobb angle was calculated from criterion vertebrae that include the first dorsal vertebra or last lumbar vertebra. In comparison with the spine screening by measuring the back surface, the estimated spinal position and the measured Cobb angle had the smaller errors. In comparison with other studies and the observer error of the manual Cobb angle, the proposed method for Cobb angle was reliable.

In comparison with the AVR measured in 3D space as a ground truth, the AVR measured by the proposed method had a smaller MAE than another study that measured the rotation angle, and compared with the rotation angle measured by observers [Wang et al., 2016]. However, in comparison with the AVR measured based on the X-ray image, the AVR measured on the estimated positions had MAE at  $2.95^\circ$ . Another study had a smaller MAE than  $1^\circ$  in comparing their ground truth with the measured one. Our result was bigger than it, but our result may not worth when considering the error of estimated positions by CNN.

About Cobb angle, the research of standard was reported that the error bigger than  $5^\circ$  is influenced to the treatment. Therefore, the error of Cobb angle should be smaller than  $5^\circ$ . On the other hand, the standard of AVR has not reported yet. Accordingly, it is unknown whether our result, MAE at 2.95, influences to the treatment or not.

An advantage of the proposed measurement methods is that the Cobb angle and the AVR were automatically measured only using the Moire image. This holds a considerable benefit considering the difficulties associated with measuring Cobb angle AVR by identifying spinal

---

features. In this respect, our method is considerably different than the conventional method.

Although our non-radiation method used Moire images, we were able to diagnose the pathological condition in the similar methods with radiation method. Consequently, our method is cost-effective, and can reduce the need of radiation method during the screening. Screens which use non-radiation methods seek to classify those suspected of demonstrating AIS in order to refer these individuals to a hospital for additional diagnosis and treatment, if indicated. Historically, these methods identify many normal students because the classification scheme is based on surface metrics. The use of our method can reduce the number of individuals suspected of demonstrating AIS by classification subdivision. Furthermore, our method is appropriate for monitoring by supplying the diagnostic index.

The proposed system is able to use for not only the screening but also a health care machine for the spine. The general screening machine functions to send the student at risk to the hospital, which actually includes many students just needs a little care like exercise. Since the proposed system provides a spine shape and a bent angle of the spine as results, the proposed system is able to function as screening machine to send student only at high risk who needs a hospital treatment as well as function as a healthcare machine to care the students at risk.

In conclusion, the proposed estimator is able to screen the spine by using only a Moire image without markers on the landmarks or the radiation exposure, but with the advantages of the Moire screening machine. It can be used in schools as well as health centers or industrial complexes where spinal screening and checks are conducted.

To increase the performance of the proposed screening system, we need to accomplish the investigation of Moire patterns corresponding to each body type. A skinny, fat or muscularity build can have specific features on the Moire image. Not only the body type but also type of scoliosis should be investigated like kyphosis called a turtleneck. While an area around a shoulder blade protrudes for the normal spine, the surface around a center of back protrudes for the spine with kyphosis. In this case, the Moire pattern has specific features decreasing

the accuracy of estimation as shown in Figure 5-9. For future works, the investigations of the body type and scoliosis type are required to approach high accuracy for the screening system.

The standard method for measuring the rotation angle, and the diagnosis criteria of scoliosis by the rotation angle are not defined yet. By establishing a diagnosis standard of criteria, the diagnosis of scoliosis can be subdivided into scoliosis types such as structural or non-structural. Moreover, it enables to implement the automatic evaluation of the spine for subdivided results. We hope that our results about the AVR can contribute for establishing the standards of the rotation angle.

---

## References

- Aaro, S., & Dahlborn, M. (1981). Estimation of vertebral rotation and the spinal and rib cage deformity in scoliosis by computer tomography. *Spine*, 6(5), 460-467.
- Adams forward bend test. (2018.6.30). [https://en.wikipedia.org/wiki/Adams\\_Forward\\_Bend\\_Test](https://en.wikipedia.org/wiki/Adams_Forward_Bend_Test)
- Altaf, F., Drinkwater, J., Phan, K., & Cree, A. K. (2017). Systematic Review of School Scoliosis Screening. *Spine deformity*, 5(5), 303-309.
- Altaf, F., Gibson, A., Dannawi, Z., & Noordeen, H. (2013). Adolescent idiopathic scoliosis. *Bmj*, 346(f2508), 1-7.
- Amendt, L. E., Ause-Ellias, K. L., Eybers, J. L., Wadsworth, C. T., Nielsen, D. H., & Weinstein, S. L. (1990). Validity and reliability testing of the Scoliometer®. *Physical therapy*, 70(2), 108-117.
- Antal, A., Katona, A., Major, P., Molnar, J., Szakaly, N., Tamás, P., & Wenzel, K. (2015). Virtually and Depth Sensor Generated Moire Pictures in Screening and Treatment of Scoliosis.
- Batouche, M. (1992, January). A knowledge based system for diagnosing spinal deformations: Moire pattern analysis and interpretation. In *Pattern Recognition. Vol. I. Conference A: Computer Vision and Applications, Proceedings., 11th IAPR International Conference on IEEE*, 591-594.
- Batouche, M., Benlamri, R., & Kholadi, M. K. (1996). A computer vision system for diagnosing scoliosis using moiré images. *Computers in Biology and Medicine*, 26(4), 339-353.
- Berryman, F., Pynsent, P., Fairbank, J., & Disney, S. (2008). A new system for measuring three-dimensional back shape in scoliosis. *European Spine Journal*, 17(5), 663-672.
- Bland, J. M., & Altman, D. (1986). Statistical methods for assessing agreement between two methods of clinical measurement. *The lancet*, 327(8476), 307-310.

- Bonnet, V., Yamaguchi, T., Dupeyron, A., Andary, S., Seilles, A., Fraisse, P., & Venture, G. (2016, June). Automatic estimate of back anatomical landmarks and 3D spine curve from a Kinect sensor. In *Biomedical Robotics and Biomechatronics (BioRob), 2016 6th IEEE International Conference on IEEE*, 924-929.
- Bunnell, W. P. (2005). Selective screening for scoliosis. *Clinical Orthopaedics and Related Research*®, 434, 40-45.
- Carlbom, I., & Paciorek, J. (1978). Planar geometric projections and viewing transformations. *ACM Computing Surveys (CSUR)*, 10(4), 465-502.
- Castro, A. P. G., Pacheco, J. D., Lourenço, C., Queirós, S., Moreira, A. H. J., Rodrigues, N. F., & Vilaça, J. L. (2017). Evaluation of spinal posture using Microsoft Kinect™: A preliminary case-study with 98 volunteers. *Porto Biomedical Journal*, 2(1), 18-22.
- Chen, H., Shen, C., Qin, J., Ni, D., Shi, L., Cheng, J. C., & Heng, P. A. (2015, October). Automatic localization and identification of vertebrae in spine CT via a joint learning model with deep neural networks. In *International Conference on Medical Image Computing and Computer-Assisted Intervention*, Springer, Cham, 515-522.
- Choi, R., Watanabe, K., & Aoki, Y. (Unpublished). Measurement of Vertebral Rotation from Moire image for Screening of adolescent Idiopathic Scoliosis
- Choi, R., Watanabe, K., Jinguji, H., Fujita, N., Ogura, Y., Demura, S., ... & Aoki, Y. (2017). CNN-based Spine and Cobb Angle Estimator Using Moire Images (Special issue on Image Processing for Life and Its Application). *IEEEJ transactions on image electronics and visual computing*, 5(2), 135-144.
- Cobb Angle. (2018.6.30). [https://en.wikipedia.org/wiki/Cobb\\_angle](https://en.wikipedia.org/wiki/Cobb_angle)
- COBB, J. R. (1948). Outlines for the study of scoliosis. *Instr Course Lect*, 5, 261-275.
- Côté, P., Kreitz, B. G., Cassidy, J. D., Dzus, A. K., & Martel, J. (1998). A study of the diagnostic accuracy and reliability of the Scoliometer and Adam's forward bend test. *Spine*, 23(7), 796-802.
- Denton, T. E., Randall, F. M., & Deinlein, D. A. (1992). The Use of Instant Moire Photographs to Reduce Exposure from Scoliosis Radiographs. *Spine*, 17(5), 509-512.
- Diers, Formetric. (2017.12.10) <http://www.diers.de/>.
- Drerup, B. (1985). Improvements in measuring vertebral rotation from the projections of the pedicles. *Journal of Biomechanics*, 18(5), 369-378.
- Drerup, B. (2014). Rasterstereographic measurement of scoliotic deformity. *Scoliosis*, 9(1), 22. DOI: 10.1186/s13013-014-0022-7.
- Drerup, B., & Hierholzer, E. (1992). Evaluation of frontal radiographs of scoliotic spines—part I

measurement of position and orientation of vertebrae and assessment of clinical shape parameters. *Journal of biomechanics*, 25(11), 1357-1362.

- Drerup, B., & Hierholzer, E. (1994). Back shape measurement using video rasterstereography and three-dimensional reconstruction of spinal shape. *Clinical Biomechanics*, 9(1), 28-36.
- Dubrofsky, E. (2009). Homography estimation. *Diplomová práce. Vancouver: Univerzita Britské Kolumbie*.
- Fedorov, A., Beichel, R., Kalpathy-Cramer, J., Finet, J., Fillion-Robin, J. C., Pujol, S., ... & Buatti, J. (2012). 3D Slicer as an image computing platform for the Quantitative Imaging Network. *Magnetic resonance imaging*, 30(9), 1323-1341.
- Forsberg, D., Lundström, C., Andersson, M., Vavruch, L., Tropp, H., & Knutsson, H. (2013). Fully automatic measurements of axial vertebral rotation for assessment of spinal deformity in idiopathic scoliosis. *Physics in Medicine & Biology*, 58(6), 1775.
- Franko, O. I., Bray, C., & Newton, P. O. (2012). Validation of a scoliotometer smartphone app to assess scoliosis. *Journal of Pediatric Orthopaedics*, 32(8), e72-e75. DOI: 10.1097/BPO.0b013e31826bb109.
- Giavarina, D., (2015), Understanding Bland Altman analysis, *Biochem Med (Zagreb)*, 25(2), pp. 141-151.
- Göçen, S., Havitçioğlu, H., & Alici, E. (1999). A new method to measure vertebral rotation from CT scans. *European Spine Journal*, 8(4), 261-265.
- Goodfellow, I., Bengio, Y., Courville, A. (2016). Deep Learning, Online publishing, 330-372. Available: <http://www.deeplearningbook.org/>
- Hackenberg, L., & Hierholzer, E. (2002). 3-D back surface analysis of severe idiopathic scoliosis by rasterstereography: comparison of rasterstereographic and digitized radiometric data. *Studies in health technology and informatics*, 86-89.
- Harrington, P. R. (1962). Treatment of scoliosis: correction and internal fixation by spine instrumentation. *JBJS*, 44(4), 591-634.
- He, K., Zhang, X., Ren, S., & Sun, J. (2016). Deep residual learning for image recognition. In *Proceedings of the IEEE conference on computer vision and pattern recognition*, 770-778.
- He, K., Zhang, X., Ren, S., & Sun, J. (2016, October). Identity mappings in deep residual networks. In *European Conference on Computer Vision*, Springer International Publishing, 630-645.
- Ho, E. K., Upadhyay, S. S., FL Chan, D. M. R. D., Hsu, L. C. S., & Leong, J. C. Y. (1993). New Methods of Measuring Vertebral Rotation from Computed Tomographic Scans: An Intraobserver and Interobserver Study on Girls with Scoliosis. *Spine*, 18(9), 1173-1177. DOI: 10.1097/00007632-199307000-00008.

- Illés, T., Tunyogi-Csapó, M., & Somoskeöy, S. (2011). Breakthrough in three-dimensional scoliosis diagnosis: significance of horizontal plane view and vertebra vectors. *European Spine Journal*, 20(1), 135-143.
- Janicki, J. A., & Alman, B. (2007). Scoliosis: Review of diagnosis and treatment. *Paediatrics & child health*, 12(9), 771-776.
- Kelm, B. M., Wels, M., Zhou, S. K., Seifert, S., Suehling, M., Zheng, Y., & Comaniciu, D. (2013). Spine detection in CT and MR using iterated marginal space learning. *Medical image analysis*, 17(8), 1283-1292.
- Kim, H. S., Ishikawa, S., Ohtsuka, Y., Shimizu, H., Shinomiya, T., & Viergever, M. A. (2001). Automatic scoliosis detection based on local centroids evaluation on moire topographic images of human backs. *IEEE transactions on medical imaging*, 20(12), 1314-1320.
- Kim, H., Ushijima, H., Tan, J. K., Ishikawa, S., Otsuka, Y., Shimizu, H., & Shinomiya, T. (2007). Spinal deformity detection from moiré topographic image based on evaluating asymmetric degree. In *World Congress on Medical Physics and Biomedical Engineering 2006*, Springer, Berlin, Heidelberg, 2308-2311.
- Klinder, T., Ostermann, J., Ehm, M., Franz, A., Kneser, R., & Lorenz, C. (2009). Automated model-based vertebra detection, identification, and segmentation in CT images. *Medical image analysis*, 13(3), 471-482.
- Knott, G., D. (2012). Interpolating cubic splines, *Springer*, 151
- Knott, P., Mardjetko, S., & Thompson, S. (2012). A comparison of automatic vs. manual detection of anatomical landmarks during surface topography evaluation using the formtric 4D system. *Scoliosis*, 7(1), O19.
- Ko, K. R., Lee, J. W., Chae, S. H., & Pan, S. B. (2015). Study on Determining Scoliosis Using Depth Image, 36-41.
- Krizhevsky, A., Sutskever, I., & Hinton, G. E. (2012). Imagenet classification with deep convolutional neural networks. In *Advances in neural information processing systems*, 1097-1105.
- Kundu, R., Lenka, P., & Chakrabarti, A. (2012, April). Cobb angle quantification for scoliosis using image processing techniques. In *IJCA Proceedings on International Conference on Recent Advances and Future Trends in Information Technology (iRAFIT'12)*, Foundation of Computer Science, 6-10
- Kunkel, M. E., Schmidt, H., & Wilke, H. J. (2010). Prediction equations for human thoracic and lumbar vertebral morphometry. *Journal of anatomy*, 216(3), 320-328.
- Kuroki, H. (2017). School Scoliosis Screening-World Trends and the Problems Encountered in Japan. *International Journal of Orthopaedics*, 4(5), 814-818.

- Lam, G. C., Hill, D. L., Le, L. H., Raso, J. V., & Lou, E. H. (2008). Vertebral rotation measurement: a summary and comparison of common radiographic and CT methods. *Scoliosis*, 3(1), 16. DOI: 10.1186/1748-7161-3-16.
- Lam, G. C., Hill, D. L., Le, L. H., Raso, J. V., & Lou, E. H. (2008). Vertebral rotation measurement: a summary and comparison of common radiographic and CT methods. *Scoliosis*, 3(1), 16.
- LeCun, Y., Bengio, Y., & Hinton, G. (2015). Deep learning. *nature*, 521(7553), 436.
- Li, M., Cheng, J., Ying, M., Ng, B., Lam, T. P., & Wong, M. S. (2015). A Preliminary Study of Estimation of Cobb's Angle from the Spinous Process Angle Using a Clinical Ultrasound Method. *Spine deformity*, 3(5), 476-482. DOI: 10.1016 /j.jspd.2015.03.001.
- Li, Q., Cai, W., Wang, X., Zhou, Y., Feng, D. D., & Chen, M. (2014, December). Medical image classification with convolutional neural network. In *Control Automation Robotics & Vision (ICARCV), 2014 13th International Conference on IEEE*, 844-848.
- Liu, X. C., Thometz, J. G., Tassone, J. C., Paulsen, L. C., & Lyon, R. M. (2003). Historical review and experience with the use of surface topographic systems in children with idiopathic scoliosis. *ISIS*, 2, 8.
- Mangone, M., Raimondi, P., Paoloni, M., Pellanera, S., Di Michele, A., Di Renzo, S., ... & Santilli, V. (2013). Vertebral rotation in adolescent idiopathic scoliosis calculated by radiograph and back surface analysis-based methods: correlation between the Raimondi method and rasterstereography. *European Spine Journal*, 22(2), 367-371.
- Melhem, E., Assi, A., El Rachkidi, R., & Ghanem, I. (2016). EOS® biplanar X-ray imaging: concept, developments, benefits, and limitations. *Journal of children's orthopaedics*, 10(1), 1-14.
- Monji, J. & Koreska, J., (unpublished) Analysis of spine rotation: a new accurate method for clinical use.
- Montgomery, F., Persson, U., Benoni, G., Willner, S., & Lindgren, B. (1990). Screening for scoliosis. A cost-effectiveness analysis. *Spine*, 15(2), 67-70.
- Parvizi, J. (2010). *High Yield Orthopaedics E-Book*. Elsevier Health Sciences.
- Patias, P., Grivas, T. B., Kaspiris, A., Aggouris, C., & Drakoutos, E. (2010). A review of the trunk surface metrics used as Scoliosis and other deformities evaluation indices. *Scoliosis*, 5(1), 12. DOI: 10.1186/1748-7161-5-12.
- Perdriolle, R., & Vidal, J. (1985). Thoracic idiopathic scoliosis curve evolution and prognosis. *Spine*, 10(9), 785-791.
- Pinheiro, A. P., Tanure, M. C., & Oliveira, A. S. (2010). Validity and reliability of a computer method to estimate vertebral axial rotation from digital radiographs. *European Spine Journal*, 19(3), 415-420.
- Placzek, J. D., & Boyce, D. A. (2016). *Orthopaedic Physical Therapy Secrets-E-Book*. Elsevier Health

Sciences.

- Pomero, V., Mitton, D., Laporte, S., de Guise, J. A., & Skalli, W. (2004). Fast accurate stereoradiographic 3D-reconstruction of the spine using a combined geometric and statistic model. *Clinical Biomechanics*, 19(3), 240-247. DOI: 10.1016/j.clinbiomech.2003.11.014.
- Ramirez, L., Durdle, N. G., Raso, V. J., & Hill, D. L. (2006). A support vector machines classifier to assess the severity of idiopathic scoliosis from surface topography. *IEEE Transactions on Information Technology in Biomedicine*, 10(1), 84-91.
- Rankine, L., Liu, X. C., Tassone, C., Lyon, R., Tarima, S., & Thometz, J. (2012). Reproducibility of newly developed spinal topography measurements for scoliosis. *The open orthopaedics journal*, 6, 226.
- Roth, H. R., Lu, L., Liu, J., Yao, J., Seff, A., Cherry, K., ... & Summers, R. M. (2016). Improving computer-aided detection using convolutional neural networks and random view aggregation. *IEEE transactions on medical imaging*, 35(5), 1170-1181.
- Ruggerone, M., & Austin, J. H. (1986). Moire topography in scoliosis: correlations with vertebral lateral curvature as determined by radiography. *Physical therapy*, 66(7), 1072-1077.
- Sardjono, T. A., Wilkinson, M. H., Veldhuizen, A. G., van Ooijen, P. M., Purnama, K. E., & Verkerke, G. J. (2013). Automatic Cobb angle determination from radiographic images. *Spine*, 38(20), E1256-E1262.
- Schmidhuber, J. (2015). Deep learning in neural networks: An overview. *Neural networks*, 61, 85-117.
- Schulte, T. L., Hierholzer, E., Boerke, A., Lerner, T., Liljenqvist, U., Bullmann, V., & Hackenberg, L. (2008). Raster stereography versus radiography in the long-term follow-up of idiopathic scoliosis. *Clinical Spine Surgery*, 21(1), 23-28.
- Screening (2018.6.30) [https://en.wikipedia.org/wiki/Screening\\_\(medicine\)](https://en.wikipedia.org/wiki/Screening_(medicine))
- Smith Neto, P., & Coelho, G. C. (2000). The Shadow Moiré method using the phase shifting technique and digital image processing: computational implementation and application to the 3D-reconstruction of a buckled plate. *Journal of the Brazilian Society of Mechanical Sciences*, 22(3), 399-409.
- Takasaki, H. (1970). Moiré topography. *Applied optics*, 9(6), 1467-1472.
- Tanee, S., & Thanapatay, D. (2017, March). Scoliosis screening using depth camera. In *Electrical Engineering Congress (iEECON), 2017 International*, IEEE, 1-4.
- Theologis, T. N., Fairbank, J. C., Turner-Smith, A. R., & Pantazopoulos, T. (1997). Early detection of progression in adolescent idiopathic scoliosis by measurement of changes in back shape with the integrated shape imaging system scanner. *Spine*, 22(11), 1223-1227.
- Thometz, J. G., Liu, X. C., Lyon, R., & Harris, G. F. (2000). Variability in three-dimensional measurements of back contour with raster stereography in normal subjects. *Journal of Pediatric*

*Orthopaedics*, 20(1), 54.

- Toshev, A., & Szegedy, C. (2014). Deeppose: Human pose estimation via deep neural networks. In *Proceedings of the IEEE Conference on Computer Vision and Pattern Recognition*, 1653-1660.
- Vrtovec, T., Pernuš, F., & Likar, B. (2009). A review of methods for quantitative evaluation of axial vertebral rotation. *European Spine Journal*, 18(8), 1079-1090. DOI: 10.1007/s00586-009-0914-z.
- Wang, Q., Li, M., Lou, E. H., Chu, W. C., Lam, T. P., Cheng, J. C., & Wong, M. S. (2016). Validity Study of Vertebral Rotation Measurement Using 3-D Ultrasound in Adolescent Idiopathic Scoliosis. *Ultrasound in medicine & biology*, 42(7), 1473-1481.
- Weinstein, S. L., Dolan, L. A., Cheng, J. C., Danielsson, A., & Morcuende, J. A. (2008). Adolescent idiopathic scoliosis. *The Lancet*, 371(9623), 1527-1537.
- Weisz, I., Jefferson, R. J., Turner-Smith, A. R., Houghton, G. R., & Harris, J. D. (1988). ISIS scanning: a useful assessment technique in the management of scoliosis. *Spine*, 13(4), 405-408.
- Yao, J., O'Connor, S. D., & Summers, R. M. (2006, April). Automated spinal column extraction and partitioning. In *Biomedical Imaging: Nano to Macro, 2006. 3rd IEEE International Symposium on*, IEEE, 390-393.
- Zhang, J., Li, H., Lv, L., & Zhang, Y. (2017). Computer-Aided Cobb Measurement Based on Automatic Detection of Vertebral Slopes Using Deep Neural Network. *International Journal of Biomedical Imaging*, 2017. 1-6.
- Zhang, J., Lou, E., Hill, D. L., Raso, J. V., Wang, Y., Le, L. H., & Shi, X. (2010). Computer-aided assessment of scoliosis on posteroanterior radiographs. *Medical & biological engineering & computing*, 48(2), 185-195.
- Zhou, S. H., McCarthy, I. D., McGregor, A. H., Coombs, R. R. H., & Hughes, S. P. F. (2000). Geometrical dimensions of the lower lumbar vertebrae—analysis of data from digitised CT images. *European Spine Journal*, 9(3), 242-248.



# Acknowledgement

First of all, I would like to thank my adviser, Yoshimitsu Aoki. He provided all environments that I need for the study, and always gave a helping hand when I needed to. In addition, I would like to thank Prof. Mitsukura, Prof. Tanaka, and Prof. Okada. I believe that your advices made my thesis improved greatly. I would like to thank Prof. Changsuk Cho who gave me many opportunities. He opened my potential, and showed new future. I would like to thank my research cooperators, Prof. Kota Watanabe at Keio hospital, Prof. Sato at Space vision Inc., and Takahashi-san at Tokyo health service association to supported my research, and gave me helpful advices. Especially, I would like to thank Prof. Kota Watanabe and teams for the data collection.

I also want to thank Ayaka Tomonari, Taiki Yamamoto, and Hashimoto Kiyoshi who have become my friends. Thanks to them, I could enjoy my life in Japan. I would like to thank my life friends, Goyo, Gihee, Minhey and Kaining who came here to give me energy every year, and Dawon (Previous ver. Jinah) who is coming. I would like to thank kimimasa Tamura, who always take care of me, and share/discuss my problems. Thanks to him, I could overcome difficulties and problems and got Ph.D finally.

Lastly, dear my parents, Hankyu Choi, Insuk Park. I truly respect your determination and patience, and sincerely thank you for believing me. My brother, sister-in-law and lovely nephew, Jonghyeon Choi, Eunhyun Lee and Hogyum Choi. Thank you for giving me lots of advices and supports whenever I have a problem in my life. I hope all of people listed here live a whole life with happiness.